Soil Dynamics and Earthquake Engineering 67 (2014) 273–289

Contents lists available at ScienceDirect

Soil Dynamics and Earthquake Engineering

journal homepage: www.elsevier.com/locate/soildyn

First-order doubly-asymptotic formulation of the direct stiffness method for elastodynamic problems

Marcelo A. Ceballos [a,b,*], Carlos A. Prato [a]

[a] Facultad de Ciencias Exactas, Físicas y Naturales, Universidad Nacional de Córdoba, Córdoba, Argentina
[b] Consejo Nacional de Investigaciones Científicas y Técnicas (CONICET), Argentina

ARTICLE INFO

Article history:
Received 25 January 2014
Received in revised form
27 July 2014
Accepted 28 September 2014

Keywords:
Layered media
Wave propagation modes
Thin-layer method
Elastodynamics
Soil–structure interaction

ABSTRACT

A first-order formulation to analyze the dynamic response of layered soil profiles is presented as an alternative to the widely used second-order thin-layer method by the direct stiffness approach, including an efficient simulation of the underlaying elastic half-space. In contrast to the thin-layer method where response is expressed through a combination of second-order propagation modes, the proposed procedure uses first-order modal parameters that have the capacity to provide a good approximation in the complete wave number domain k, including the exact stiffness values for $k=0$ and $k\to\infty$, thus justifying its designation of doubly-asymptotic. This feature allows obtaining the exact soil profile response for static loads, while the proposed treatment of the elastic half-space reproduces naturally the radiation condition without a need of artificial damping. The capacity of the proposed formulation to solve elastodynamic problems is assessed by comparing its results with those of exact solutions available in the literature, and numerical solutions of rigid disks supported on the surface of different soil profiles.

1. Introduction

The direct stiffness method provides the basis for both the thin-layer method and for the new proposed method here, designated as first-order doubly-asymptotic formulation (FODAF). The exact stiffness matrices in the wave number domain for a finite stratum and for a half-space were given by Kausel and Roesset [1]. Calculation of the profile response by these methods is carried out for each frequency by transforming the excitation from the space domain to the wave number domain, calculating the displacements through the stiffness matrix of the soil profile and then applying the inverse transform into the space domain. The Hankel Transform allows calculating the response in cylindrical coordinates from the wave number domain to the spatial domain. The numerical implementations of this transform lead to inaccuracies due to singularities of the integrand that may be reduced by refining the discretization in the wave number k at an increased computational effort.

The thin-layer method (TLM) described in detail by Kausel [2] and Park [3] approximates the exact stiffness of a layer by the direct method through matrices that are independent of the wave number. The main advantage of this method lies in approximating the transcendental form of stiffness coefficients by algebraic expressions leading to a solution expressed in terms of eigenvalues associated with propagation modes of the soil profile. Such representation allows an analytical transformation into the space domain without additional loss of accuracy. In this approach the layers stiffness coefficients for wave numbers which tend to infinity are proportional to k^2 while the exact stiffness coefficients vary with k. This characteristic brings in the shortcoming that the method is not rigorously capable of representing static solutions of the soil profile. Representation of an underlying half-space in the thin-layer method is done by incorporating additional strata of increasing thickness up to a total thickness of 1.5 times the wave length for each frequency, and vertical and horizontal dashpots at the base of the lowest stratum as an approximation to the consistent boundary conditions as presented by Lysmer and Kuhlemeyer [4]. This last approach is only effective for plane and axisymmetric models according to Lin et al. [5], so that Oliveira Barbosa et al. [6] recently provided an improved approximation based on the perfectly matched layer technique (PML).

The first-order formulation proposed here relies on an expansion of the exact coefficients of the layer stiffness matrix up to the first power of k generating two independent matrices with respect to the wave number. In this way, the coefficients of the formulation are proportional to k for wave numbers tending to infinity as in the exact solution. The modal parameters result of the

* Corresponding author at: Facultad de Ciencias Exactas, Físicas y Naturales, Universidad Nacional de Córdoba, Córdoba, Argentina. Tel.: +54 351 5353800x718.
E-mail addresses: mceballo@efn.uncor.edu (M.A. Ceballos), prato_carlos@yahoo.com (C.A. Prato).

http://dx.doi.org/10.1016/j.soildyn.2014.09.015
0267-7261/

first-order in contrast to thin-layer method where they derive from second order matrices. Addition of auxiliary degrees of freedom (d.o.f.) to the stiffness matrices allows a good match with the exact coefficients in the wave number domain. These auxiliary d.o.f. are used to enlarge the modal model, and from the point of view of modal analysis can be considered as secondary or slave d.o.f., which once condensed to the primary or master d.o.f. allow to reproduce adequately the variations of the stiffness coefficients with respect to the wave number.

On the other hand, an experimental modal analysis technique is used to adjust the exact stiffness coefficients of the half-space through first-order modal parameters. The half-space modal model is then transformed into physical matrices that can be assembled with the matrices for the soil layers. Matching of the stiffness coefficients of the half-space is carried out both for real and imaginary components allowing a correct simulation of the radiation process and of the solution for the static cases. As a result, this formulation turns out to be doubly-asymptotic since it tends to the exact solution both when the wave number tends to zero and to infinity. Such feature is of interest in order to represent the soil profile response at low frequencies, including the static case, while retaining the advantage of the thin-layer method of the exact modal transformation from the wave number domain to the spacial domain. In addition, the foregoing formulation does not require artificial damping to avoid numerical problems. If required, material damping of the strata may be accounted for by adding it to the eigenvalues of the complete soil profile. Main issues related to the calculation of integrals of the Hankel Transform that arise in this formulation are discussed in the paper.

2. Direct stiffness method

Fig. 1 shows load and displacement components at the interfaces of the jth layer according to terminology adopted by Kausel and Roesset [1]. Cylindrical coordinates will be used here, although resulting matrices both for strata and for the half-space are also valid for plane wave fronts in cartesian coordinates.

Load vector P_j for each interface is transformed from the time domain t to the frequency domain ω through the Fourier Transform, azimutal coordinate θ is expressed in terms of Fourier series through integer numbers μ, and radial coordinate ρ is transformed to the wave number domain k by the Hankel Transform:

$$\overline{P}_j(k,\mu,\omega) = a_\mu \int_0^\infty \rho\, C_\mu \int_0^{2\pi} T_\mu \int_{-\infty}^{\infty} P_j(\rho,\theta,t)\, e^{-i\omega t} dt\, d\theta\, d\rho \tag{1}$$

$$a_\mu = \begin{cases} 1/2\pi & \text{if} \quad \mu = 0 \\ 1/\pi & \text{if} \quad \mu \neq 0 \end{cases} \tag{2}$$

$$C_\mu = \begin{bmatrix} \frac{d}{d(k\rho)} J_\mu(k\rho) & \frac{\mu}{k\rho} J_\mu(k\rho) & 0 \\ \frac{\mu}{k\rho} J_\mu(k\rho) & \frac{d}{d(k\rho)} J_\mu(k\rho) & 0 \\ 0 & 0 & -J_\mu(k\rho) \end{bmatrix} \tag{3}$$

$$T_\mu = \begin{cases} \text{diag}\left[\cos(\mu\theta) \;\; -\sin(\mu\theta) \;\; \cos(\mu\theta)\right] : \text{symmetric loads respect to } x-\text{axis} \\ \text{diag}\left[\sin(\mu\theta) \;\; \cos(\mu\theta) \;\; \sin(\mu\theta)\right] : \text{anti}-\text{symmetric loads respect to } x-\text{axis} \end{cases} \tag{4}$$

where $J_\mu(k\rho)$ is the Bessel function of μth order.

Force–displacement relations for a layer are expressed as:

$$K_j^{st} \overline{U}_j^{st} = \overline{P}_j^{st} \tag{5}$$

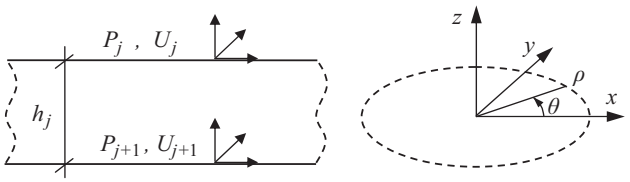

Fig. 1. Load and displacement components of the jth layer.

or:

$$\begin{bmatrix} K_{jj} & K_{jj+1} \\ K_{j+1j} & K_{j+1j+1} \end{bmatrix} \begin{bmatrix} \overline{U}_j \\ \overline{U}_{j+1} \end{bmatrix} = \begin{bmatrix} \overline{P}_j \\ \overline{P}_{j+1} \end{bmatrix} \tag{6}$$

In cylindrical coordinates this last expression takes the form:

$$\begin{bmatrix} K_{11} & 0 & K_{13} & K_{14} & 0 & K_{16} \\ 0 & K_{22} & 0 & 0 & K_{25} & 0 \\ K_{13} & 0 & K_{33} & -K_{16} & 0 & K_{36} \\ K_{14} & 0 & -K_{16} & K_{11} & 0 & -K_{13} \\ 0 & K_{25} & 0 & 0 & K_{22} & 0 \\ K_{16} & 0 & K_{36} & -K_{13} & 0 & K_{33} \end{bmatrix} \begin{bmatrix} \overline{u}_\rho^j \\ \overline{u}_\theta^j \\ \overline{u}_z^j \\ \overline{u}_\rho^{j+1} \\ \overline{u}_\theta^{j+1} \\ \overline{u}_z^{j+1} \end{bmatrix} = \begin{bmatrix} \overline{\tau}_{\rho z}^j \\ \overline{\tau}_{\theta z}^j \\ \overline{\sigma}_z^j \\ \overline{\tau}_{\rho z}^{j+1} \\ \overline{\tau}_{\theta z}^{j+1} \\ \overline{\sigma}_z^{j+1} \end{bmatrix} \tag{7}$$

where the degrees of freedom ρ and z (*SV-P* waves) are coupled, while d.o.f. θ (*SH* waves) is decoupled from the other ones.

The displacement vector for the complete profile is obtained as:

$$\overline{U} = K^{-1}\overline{P} = F\,\overline{P} \tag{8}$$

where K represents the stiffness matrix of the profile obtained by assembling the individual layers and half-space matrices, while F represents the flexibility matrix of the soil profile.

The inverse transform to the space-time domain of the displacements obtained from Eq. (8) is carried out by:

$$U_j = \sum_{\mu=0}^{\infty} T_\mu \int_0^\infty k\, C_\mu \int_{-\infty}^{\infty} \overline{U}_j\, e^{i\omega t} d\omega\, dk \tag{9}$$

The stiffness matrices in a non-dimensional form associated with the direct stiffness method are presented in what follows.

2.1. Layer stiffness matrices

The layer stiffness matrix for the d.o.f. associated with *SV-P* waves (Rayleigh modes) may be expressed as:

$$K_R^{st} = \omega\overline{\rho} V_S\, \overline{K}_R^{st} \tag{10}$$

$$\overline{K}_R^{st} = \begin{bmatrix} \overline{K}_{11} & \overline{K}_{13} & \overline{K}_{14} & \overline{K}_{16} \\ \overline{K}_{13} & \overline{K}_{33} & -\overline{K}_{16} & \overline{K}_{36} \\ \overline{K}_{14} & -\overline{K}_{16} & \overline{K}_{11} & -\overline{K}_{13} \\ \overline{K}_{16} & \overline{K}_{36} & -\overline{K}_{13} & \overline{K}_{33} \end{bmatrix} \tag{11}$$

$$\begin{aligned} \overline{K}_{11} &= \kappa(1-s^2)\tfrac{(T_s - rsT_r)}{Ds} \\ \overline{K}_{33} &= \kappa(1-s^2)\tfrac{(T_r - rsT_s)}{Dr} \\ \overline{K}_{14} &= \kappa(1-s^2)\tfrac{(rsT_rS_s - T_sS_r)}{Ds} \\ \overline{K}_{36} &= \kappa(1-s^2)\tfrac{(rsT_sS_r - T_rS_s)}{Dr} \\ \overline{K}_{13} &= \kappa(1-s^2)\tfrac{(1 - S_rS_s - rsT_rT_s)}{D} - \kappa(1+s^2) \\ \overline{K}_{16} &= \kappa(1-s^2)\tfrac{(S_r - S_s)}{D} \end{aligned} \tag{12}$$

$$D = 2(S_rS_s - 1) + \left(\frac{1}{rs} + rs\right)T_rT_s \tag{13}$$

$$\begin{aligned} T_r &= \tanh(r\kappa\eta) \quad T_s = \tanh(s\kappa\eta) \\ S_r &= \operatorname{sech}(r\kappa\eta) \quad S_s = \operatorname{sech}(s\kappa\eta) \end{aligned} \tag{14}$$

$$r=\sqrt{1-\frac{\alpha^2}{\kappa^2}} \quad s=\sqrt{1-\frac{1}{\kappa^2}} \quad \alpha=\sqrt{\frac{1/2-\nu}{1-\nu}} \tag{15}$$

$$\kappa=\frac{k\,Vs}{\omega} \qquad \eta=\frac{h\,\omega}{Vs} \tag{16}$$

where ω is the analysis frequency, $\overline{\rho}$ is the layer mass density, V_S is the shear wave velocity, ν is the Poisson coefficient, k and κ represent the dimensional and non-dimensional wave number, respectively, while h and η are the layer thickness in dimensional and non-dimensional form.

The layer stiffness matrix for the d.o.f. associated with the *SH* waves (Love modes) may be expressed as:

$$K_L^{st}=\omega\overline{\rho}V_S\,\overline{K}_L^{st} \tag{17}$$

$$\overline{K}_L^{st}=\begin{bmatrix}\overline{K}_{22} & \overline{K}_{25}\\ \overline{K}_{25} & \overline{K}_{22}\end{bmatrix} \tag{18}$$

$$\overline{K}_{22}=s\kappa\coth(s\kappa\eta) \quad \overline{K}_{25}=-s\kappa\,\mathrm{csch}(s\kappa\eta) \tag{19}$$

2.2. Half-space stiffness matrices

The stiffness matrix of the half-space for *SV-P* waves is expressed as:

$$K_R^{hs}=\omega\overline{\rho}V_S\,\overline{K}_R^{hs} \tag{20}$$

$$\overline{K}_R^{hs}=\frac{\kappa}{(1-rs)}\begin{bmatrix}r(1-s^2) & 2rs-1-s^2\\ 2rs-1-s^2 & s(1-s^2)\end{bmatrix} \tag{21}$$

and that for *SH* waves is:

$$K_L^{hs}=\omega\overline{\rho}V_S\,\overline{K}_L^{hs} \tag{22}$$

$$\overline{K}_L^{hs}=s\,\kappa \tag{23}$$

Taking limits is required to obtain the stiffness coefficients of layers or the half-space in all cases when $\omega=0$ and/or $k=0$ as described in [1].

3. First-order doubly-asymptotic formulation (FODAF)

The general form of the approximation proposed herein for the layer stiffness matrices both for *SV-P* and *SH* waves may be written in a kind of "nested" or "fractal" matrix representation:

$$\begin{aligned}\tilde{K}_{R/L}^{st}&=K_0+\kappa K_1-\kappa^2\tilde{K}_I^{-1}\\ \tilde{K}_I&=K_2+\kappa K_3-\kappa^2\tilde{K}_{II}^{-1}\\ \tilde{K}_{II}&=K_4+\kappa K_5-\kappa^2\tilde{K}_{III}^{-1}\\ \tilde{K}_{III}&=K_6+\kappa K_7\ldots\end{aligned} \tag{24}$$

where $\tilde{K}_{R/L}^{st}$ represents a generic approximation for both $\overline{K}_R^{st}$ and $\overline{K}_L^{st}$. An equivalent matrix form for this representation, known as "companion" matrix form in the field of experimental modal analysis, consists of two matrices that are independent of the wave number, retaining the same degree of accuracy:

$$\tilde{K}_{R/L}^{st}=\left(I_n\left(K_A^{st}+\kappa K_B^{st}\right)^{-1}I_n^T\right)^{-1} \tag{25}$$

$$I_n=\begin{bmatrix}I & 0 & 0 & \cdots & 0\end{bmatrix} \tag{26}$$

$$K_A^{st}=\left[\begin{array}{c|ccc:c}K_0 & 0 & 0 & \vdots & 0\\ \hline 0 & K_2 & 0 & \vdots & 0\\ 0 & 0 & K_4 & \vdots & 0\\ \cdots & \cdots & \cdots & \ddots & \cdots\\ 0 & 0 & 0 & \vdots & K_{2n-2}\end{array}\right]\begin{matrix}\}\ \text{physical d.o.f.'s}\\ \left.\begin{matrix}\\ \\ \\ \\ \\ \end{matrix}\right\}\ \text{auxiliary d.o.f.'s}\end{matrix}$$

$$\underbrace{\text{phy.}}\quad\underbrace{\text{auxiliary d.o.f.'s}} \tag{27}$$

$$K_B^{st}=\left[\begin{array}{c|ccc:c}K_1 & I & 0 & \vdots & 0\\ \hline I & K_3 & I & \vdots & 0\\ 0 & I & K_5 & \vdots & 0\\ \cdots & \cdots & \cdots & \ddots & \cdots\\ 0 & 0 & 0 & \vdots & K_{2n-1}\end{array}\right]\begin{matrix}\}\ \text{physical d.o.f.'s}\\ \left.\begin{matrix}\\ \\ \\ \\ \\ \end{matrix}\right\}\ \text{auxiliary d.o.f.'s}\end{matrix}$$

$$\underbrace{\text{phy.}}\quad\underbrace{\text{auxiliary d.o.f.'s}} \tag{28}$$

In this way, the layer flexibility matrices takes the standard form for first-order systems:

$$\tilde{F}_{R/L}^{st}=\left(\tilde{K}_{R/L}^{st}\right)^{-1}=I_n\left(K_A^{st}+\kappa K_B^{st}\right)^{-1}I_n^T \tag{29}$$

The parameter n represents the number of times that the d.o.f.'s of the layer are to be increased with auxiliary d.o.f.'s. The first four d.o.f.'s of matrices K_A^{st} and K_B^{st} for *SV-P* waves, and the first two d.o.f.'s of those matrices for *SH* waves represent the physical d.o.f.'s of the layer, to be assembled with those of other layers to form the matrices K_A and K_B of the complete soil profile. The auxiliary d.o.f.'s can be considered as "internal" d.o.f.'s of each layer so they are not affected by the boundary conditions or to assembling with the d.o.f.'s of other strata.

3.1. Layer stiffness matrices

The layer stiffness matrix for *SV-P* waves turns out to be nearly singular for small values of κ due to this matrix must satisfy the rigid body modes condition, and for this reason it is advantageous to provide a good match in this range. Therefore, the sub-matrices K_i from expressions (27) and (28) are obtained by equating the exact layer matrices given by Eqs. (11) and (18) and their derivatives valued at $\kappa=0$ with the proposed approximation of Eq. (24) and its respective derivatives. For *SV-P* waves, the exact layer matrix and the first derivatives result in the form:

$$\overline{K}_R^{st}\big|_{\kappa=0}=\overline{K}_{R,0}^{st}=\begin{bmatrix}k_{11}^0 & 0 & k_{14}^0 & 0\\ 0 & k_{33}^0 & 0 & k_{36}^0\\ k_{14}^0 & 0 & k_{11}^0 & 0\\ 0 & k_{36}^0 & 0 & k_{33}^0\end{bmatrix} \tag{30}$$

$$\overline{K}_R^{st\prime}\big|_{\kappa=0}=\overline{K}_{R,1}^{st}=\begin{bmatrix}0 & k_{13}^1 & 0 & k_{16}^1\\ k_{13}^1 & 0 & -k_{16}^1 & 0\\ 0 & -k_{16}^1 & 0 & -k_{13}^1\\ k_{16}^1 & 0 & -k_{13}^1 & 0\end{bmatrix} \tag{31}$$

$$\overline{K}_R^{st\,''}\Big|_{\kappa=0} = \overline{K}_{R,2}^{st} = \begin{bmatrix} k_{11}^2 & 0 & k_{14}^2 & 0 \\ 0 & k_{33}^2 & 0 & k_{36}^2 \\ k_{14}^2 & 0 & k_{11}^2 & 0 \\ 0 & k_{36}^2 & 0 & k_{33}^2 \end{bmatrix} \tag{32}$$

$$\overline{K}_R^{st\,'''}\Big|_{\kappa=0} = \overline{K}_{R,3}^{st} = \begin{bmatrix} 0 & k_{13}^3 & 0 & k_{16}^3 \\ k_{13}^3 & 0 & -k_{16}^3 & 0 \\ 0 & -k_{16}^3 & 0 & -k_{13}^3 \\ k_{16}^3 & 0 & -k_{13}^3 & 0 \end{bmatrix} \tag{33}$$

where

$$\begin{cases} k_{11}^0 = \cot(\eta) & k_{14}^0 = -\csc(\eta) \\ k_{33}^0 = \cot(\alpha\eta)/\alpha & k_{36}^0 = -\csc(\alpha\eta)/\alpha \end{cases} \tag{34}$$

$$\begin{cases} k_{13}^1 = (\csc(\eta)\csc(\alpha\eta) - \cot(\eta)\cot(\alpha\eta))/\alpha - 2 \\ k_{16}^1 = (\cot(\eta)\csc(\alpha\eta) - \csc(\eta)\cot(\alpha\eta))/\alpha \end{cases} \tag{35}$$

$$\begin{cases} k_{11}^2 = \frac{2\sin(\alpha\eta)\cos(\alpha\eta)(1+\cos(\eta)^2)+\alpha(\eta+\sin(\eta)\cos(\eta))\sin(\alpha\eta)^2-4\sin(\alpha\eta)\cos(\eta)}{\alpha\sin(\eta)^2\sin(\alpha\eta)^2} \\ k_{14}^2 = \frac{2\sin(\alpha\eta)(1+\cos(\eta)^2)-\alpha(\sin(\eta)+\eta\cos(\eta))\sin(\alpha\eta)^2-4\sin(\alpha\eta)\cos(\eta)\cos(\alpha\eta)}{\alpha\sin(\eta)^2\sin(\alpha\eta)^2} \\ k_{33}^2 = \frac{2\alpha\sin(\eta)\cos(\eta)(1+\cos(\alpha\eta)^2)+(\alpha\eta+\sin(\alpha\eta)\cos(\alpha\eta))\sin(\eta)^2-4\alpha\sin(\eta)\cos(\alpha\eta)}{\alpha^3\sin(\eta)^2\sin(\alpha\eta)^2} \\ k_{36}^2 = \frac{2\alpha\sin(\eta)(1+\cos(\alpha\eta)^2)-(\sin(\alpha\eta)+\alpha\eta\cos(\alpha\eta))\sin(\eta)^2-4\alpha\sin(\eta)\cos(\eta)\cos(\alpha\eta)}{\alpha^3\sin(\eta)^2\sin(\alpha\eta)^2} \end{cases} \tag{36}$$

$$\overline{K}_L^{st\,'''}\Big|_{\kappa=0} = \overline{K}_{L,3}^{st} = \begin{bmatrix} 0 & 0 \\ 0 & 0 \end{bmatrix} \tag{41}$$

$$\overline{K}_L^{st\ iv}\Big|_{\kappa=0} = \overline{K}_{L,4}^{st} = \begin{bmatrix} k_{22}^4 & k_{25}^4 \\ k_{25}^4 & k_{22}^4 \end{bmatrix} \tag{42}$$

$$\overline{K}_L^{st\ v}\Big|_{\kappa=0} = \overline{K}_{L,5}^{st} = \begin{bmatrix} 0 & 0 \\ 0 & 0 \end{bmatrix} \tag{43}$$

$$\overline{K}_L^{st\ vi}\Big|_{\kappa=0} = \overline{K}_{L,6}^{st} = \begin{bmatrix} k_{22}^6 & k_{25}^6 \\ k_{25}^6 & k_{22}^6 \end{bmatrix} \tag{44}$$

$$\overline{K}_L^{st\ vii}\Big|_{\kappa=0} = \overline{K}_{L,7}^{st} = \begin{bmatrix} 0 & 0 \\ 0 & 0 \end{bmatrix} \tag{45}$$

where

$$\begin{cases} k_{22}^0 = \cos(\eta)/\sin(\eta) \\ k_{25}^0 = -1/\sin(\eta) \end{cases} \tag{46}$$

$$\begin{cases} k_{22}^2 = (\eta - \sin(\eta)\cos(\eta))/\sin(\eta)^2 \\ k_{25}^2 = (\sin(\eta) - \eta\cos(\eta))/\sin(\eta)^2 \end{cases} \tag{47}$$

$$\begin{cases} k_{22}^4 = 3\left(\cos(\eta)(2\eta^2 - \sin(\eta)^2) - \eta\sin(\eta)\right)/\sin(\eta)^3 \\ k_{25}^4 = 3\left((1+\eta^2)\sin(\eta)^2 + \eta\sin(\eta)\cos(\eta) - 2\eta^2\right)/\sin(\eta)^3 \end{cases} \tag{48}$$

$$\begin{cases} k_{13}^3 = \frac{3\left(8\alpha\cos(\eta)\cos(\alpha\eta)+(1+\alpha^2)\sin(\eta)\sin(\alpha\eta)(1-\cos(\eta)\cos(\alpha\eta))-\cdots\right.}{\left.2\alpha\left(1+\cos(\eta)^2\right)\left(1+\cos(\alpha\eta)^2\right)-\alpha\eta(\sin(\eta)-\alpha\sin(\alpha\eta))(\cos(\eta)-\cos(\alpha\eta))\right)}{\alpha^3\sin(\eta)^2\sin(\alpha\eta)^2} \\ k_{16}^3 = \frac{3\left(4\alpha\cos(\alpha\eta)\left(1+\cos(\eta)^2\right)+(1+\alpha^2)\sin(\eta)\sin(\alpha\eta)(\cos(\eta)-\cos(\alpha\eta))-\cdots\right.}{\left.4\alpha\cos(\eta)\left(1+\cos(\alpha\eta)^2\right)-\alpha\eta(\sin(\eta)-\alpha\sin(\alpha\eta))(1-\cos(\eta)\cos(\alpha\eta))\right)}{\alpha^3\sin(\eta)^2\sin(\alpha\eta)^2} \end{cases} . \tag{37}$$

and $'$ denotes derivative with respect to κ. Since the complexity of these coefficients increases rapidly with the derivation order, to simplify the resulting expressions they are expanded in η. Consequently, and for the purpose of maintaining the expansion validity, a maximum value of this parameter is defined from which the layer must be subdivided into sub-layers as is done in the thin-layer method. Such maximum value adopted in numerical examples presented later is $\eta=\pi/2$. At the same time, the proposed expansion allows to avoid numerical problems associated with inherent limitations of the computer accuracy that arise during the valuation of the exact expressions.

In the case of *SH* waves, the exact layer matrix and its first derivatives for $\kappa=0$ are:

$$\overline{K}_L^{st}\Big|_{\kappa=0} = \overline{K}_{L,0}^{st} = \begin{bmatrix} k_{22}^0 & k_{25}^0 \\ k_{25}^0 & k_{22}^0 \end{bmatrix} \tag{38}$$

$$\overline{K}_L^{st\prime}\Big|_{\kappa=0} = \overline{K}_{L,1}^{st} = \begin{bmatrix} 0 & 0 \\ 0 & 0 \end{bmatrix} \tag{39}$$

$$\overline{K}_L^{st\,''}\Big|_{\kappa=0} = \overline{K}_{L,2}^{st} = \begin{bmatrix} k_{22}^2 & k_{25}^2 \\ k_{25}^2 & k_{22}^2 \end{bmatrix} \tag{40}$$

$$\begin{cases} k_{22}^6 = 15\left(2\eta^3(1+2\cos(\eta)^2) - 3(\eta+\sin(\eta)\cos(\eta))\sin(\eta)^2\right)/\sin(\eta)^4 \\ k_{25}^6 = 15\left(3\sin(\eta)^2(\sin(\eta)+\eta\cos(\eta)) - \eta^3\cos(\eta)(5+\cos(\eta)^2)\right)/\sin(\eta)^4 \end{cases} \tag{49}$$

Sub-matrices K_i of the approximation proposed in Eq. (24) are obtained in the following form:

$$\begin{aligned} \tilde{K}_{R/L}^{st}\Big|_{\kappa=0} &= \overline{K}_{R/L,0}^{st} = K_0 && \Rightarrow \quad K_0 = \overline{K}_{R/L,0}^{st} \\ \tilde{K}_{R/L}^{st\prime}\Big|_{\kappa=0} &= \overline{K}_{R/L,1}^{st} = K_1 && \Rightarrow \quad K_1 = \overline{K}_{R/L,1}^{st} \\ \tilde{K}_{R/L}^{st\,''}\Big|_{\kappa=0} &= \overline{K}_{R/L,2}^{st} = -2K_2^{-1} && \Rightarrow \quad K_2 = -2\left(\overline{K}_{R/L,2}^{st}\right)^{-1} \\ \tilde{K}_{R/L}^{st\,'''}\Big|_{\kappa=0} &= \overline{K}_{R/L,3}^{st} = 6K_2^{-1}K_3K_2^{-1} && \Rightarrow \quad K_3 = 1/6\times K_2\overline{K}_{R/L,3}^{st}K_2 \\ \tilde{K}_{R/L}^{st\ iv}\Big|_{\kappa=0} &= -24K_2^{-1}\left(K_3K_2^{-1}K_3+K_4^{-1}\right)K_2^{-1} && \Rightarrow \quad K_4 = \ldots \end{aligned} \tag{50}$$

A practical and numerically efficient calculation of sub-matrices K_i for high order derivatives consists in gradually completing matrices K_A and K_B from Eq. (25) taking into account that the terms where these sub-matrices appear for the first time present

the following pattern:

$$\begin{aligned}
&\tilde{K}^{st\ iv}_{R/L}\big|_{\kappa=0} = \ldots - 4!K_2^{-1}K_4^{-1}K_2^{-1} && \Rightarrow \quad K_4 = \ldots\\
&\tilde{K}^{st\ v}_{R/L}\big|_{\kappa=0} = \ldots + 5!K_2^{-1}K_4^{-1}K_5K_4^{-1}K_2^{-1} && \Rightarrow \quad K_5 = \ldots\\
&\tilde{K}^{st\ vi}_{R/L}\big|_{\kappa=0} = \ldots - 6!K_2^{-1}K_4^{-1}K_6^{-1}K_4^{-1}K_2^{-1} && \Rightarrow \quad K_6 = \ldots\\
&\tilde{K}^{st\ vii}_{R/L}\big|_{\kappa=0} = \ldots + 7!K_2^{-1}K_4^{-1}K_6^{-1}K_7K_6^{-1}K_4^{-1}K_2^{-1} && \Rightarrow \quad K_7 = \ldots\\
&\tilde{K}^{st\ viii}_{R/L}\big|_{\kappa=0} = \ldots - 8!K_2^{-1}K_4^{-1}K_6^{-1}K_8^{-1}K_6^{-1}K_4^{-1}K_2^{-1} && \Rightarrow \quad K_8 = \ldots
\end{aligned} \tag{51}$$

The proposed formulation implies by definition the exact values for $\kappa=0$. It also leads to exact values for $\kappa\to\infty$ if the last sub-matrix of the approximation is calculated, depending on the adopted value of n, as follows:

$$\begin{aligned}
&n=3 \to K_5 = (K_3 - (K_1 - \overline{K}^{st}_{R/L,\infty})^{-1})^{-1}\\
&n=4 \to K_7 = (K_5 - (K_3 - (K_1 - \overline{K}^{st}_{R/L,\infty})^{-1})^{-1})^{-1}\\
&n=5 \to K_9 = (K_7 - (K_5 - (K_3 - (K_1 - \overline{K}^{st}_{R/L,\infty})^{-1})^{-1})^{-1})^{-1}
\end{aligned} \tag{52}$$

where

$$\overline{K}^{st}_{R,\infty} = \left(\kappa^{-1}\overline{K}^{st}_{R}\right)\Big|_{\kappa\to\infty} = \begin{bmatrix} k^{\infty}_{11} & k^{\infty}_{13} & 0 & 0\\ k^{\infty}_{13} & k^{\infty}_{33} & 0 & 0\\ 0 & 0 & k^{\infty}_{11} & -k^{\infty}_{13}\\ 0 & 0 & -k^{\infty}_{13} & k^{\infty}_{33} \end{bmatrix}$$

$$\overline{K}^{st}_{L,\infty} = \left(\kappa^{-1}\overline{K}^{st}_{L}\right)\Big|_{\kappa\to\infty} = \begin{bmatrix} k^{\infty}_{22} & 0\\ 0 & k^{\infty}_{22} \end{bmatrix} \tag{53}$$

and

$$k^{\infty}_{11} = k^{\infty}_{33} = \frac{2}{(1+\alpha^2)} \quad k^{\infty}_{13} = \frac{-2\alpha^2}{(1+\alpha^2)} \quad k^{\infty}_{22} = 1 \tag{54}$$

In this way, this formulation turns out to be doubly-asymptotic. Fig. 2 shows the degree of matching achieved with this procedure for $\nu=1/3$, together with the curves obtained using the thin-layer method (TLM), after rescaling the stiffness coefficients as follows:

$$\begin{aligned}
&\overline{\overline{K}}^{st}_{R} = \Upsilon_R^{-1/2}\overline{K}^{st}_{R}\Upsilon_R^{-1/2}\\
&\overline{\overline{K}}^{st}_{L} = \Upsilon_L^{-1/2}\overline{K}^{st}_{L}\Upsilon_L^{-1/2}
\end{aligned} \tag{55}$$

with

$$\begin{aligned}
&\Upsilon_R = diag\left([(k^0_{11}+\kappa k^{\infty}_{11}) \quad (k^0_{33}+\kappa k^{\infty}_{33}) \quad (k^0_{11}+\kappa k^{\infty}_{11}) \quad (k^0_{33}+\kappa k^{\infty}_{33})]\right)\\
&\Upsilon_L = diag\left([(k^0_{22}+\kappa k^{\infty}_{22}) \quad (k^0_{22}+\kappa k^{\infty}_{22})]\right)
\end{aligned} \tag{56}$$

The degree of approximation shown in Fig. 2 is also representative of that obtained for other values of the Poisson coefficient. Moreover, plotting these curves for different values of the non-dimensional thickness shows that the stiffness components are virtually independent of the thickness for $\eta<0.1$ by assigning the abscissa the value $\kappa\eta$. Even though the approximation is satisfactory even for much higher thicknesses, it seems advisable to take $\eta=\pi/2$ as upper bound before dividing into sub-layers since the exact flexibility coefficients present abrupt variations after this value.

The proposed formulation for the stiffness coefficients departs from the exact solution only for high wave numbers, and therefore may lead to inaccuracies only in rather special situations. The critical issue regarding the need for subdividing the thickness of layers occurs when the loaded area is small compared with the layer thickness, as is the case of point loads. In any event, as shown in what follows, the requirements for refinement of layers in the proposed formulation are less restrictive than in the thin-layer method. In fact, in the case of a point load applied on a layer supported on a rigid half-space, the proposed formulation does not present any appreciable difference with the exact solution except in the vicinity of the applied load.

Table 1 shows the $\kappa\eta$ values below which the thin-layered method and the proposed formulation depart less than 1% from the exact coefficients. It is observed that for the first few coefficients, particularly those of the main diagonal, the proposed formulation is notoriously more accurate than the thin-layer method.

Fig. 2 shows that convergence of the proposed formulation oscillates for increasing values of n and that for $n=4$ the approximation is satisfactory in the complete range of wave numbers. On this basis, it is concluded that $n=4$ is a recommendable value for the present formulation, which is used in all numerical examples presented here.

3.2. Half-space stiffness matrices

The half-space stiffness matrices are obtained by adjusting the exact flexibility coefficients in wave number domain through an experimental modal analysis technique. Ceballos and Prato [7] has developed a technique to obtain second-order stiffness matrices for the half-space that can be assembled with the layer matrices of the thin-layer method for calculating the eigenvalues of the complete profile. In that approach, both real and imaginary flexibility components were adjusted adding a small amount of hysteretic damping. This approximation allows to consider the radiation damping through the half-space, but does not provide satisfactory results for the response in the range of relatively low exciting frequencies.

In the present work, the adjustment of the half-space flexibility is performed with the same technique used in [7] but with first-order modal parameters and without addition of material damping. These parameters are defined so as to enforce that the flexibility coefficients tend to the exact values when the wave number κ tends both to zero and to infinity. In this way, the stiffness matrix of the complete soil profile retains the doubly-asymptotic characteristic.

As a first step, the unbounded amplitudes of the half-space flexibility matrix are eliminated discounting the exact Rayleigh wave propagation mode. This mode is added to the modal basis in the final stage of the adjustment process. Using auxiliary degrees of freedom as in the case of the layer matrices allows to obtain a square matrix of mode shapes. The half-space modal matrices are then transformed into physical matrices that can be assembled directly with the layer matrices obtained in the previous section.

The procedure described in what follows should be applied for each value of interest of Poisson coefficient ν in order to construct a data-base with the parameters adjusted in each instance.

3.2.1. SV-P waves

The Rayleigh waves propagation mode in a homogeneous half-space may be derived form the flexibility matrix obtained inverting the stiffness matrix of Eq. (21):

$$\overline{F}^{hs}_{R} = \left(\overline{K}^{hs}_{R}\right)^{-1} = \frac{1}{\kappa(4rs-s^4-2s^2-1)}\begin{bmatrix} s(1-s^2) & 1+s^2-2rs\\ 1+s^2-2\,r\,s & r(1-s^2) \end{bmatrix} \tag{57}$$

The wave number associated with the Rayleigh mode $\kappa_0=V_S/V_R$ is obtained as the single root of the common denominator of the

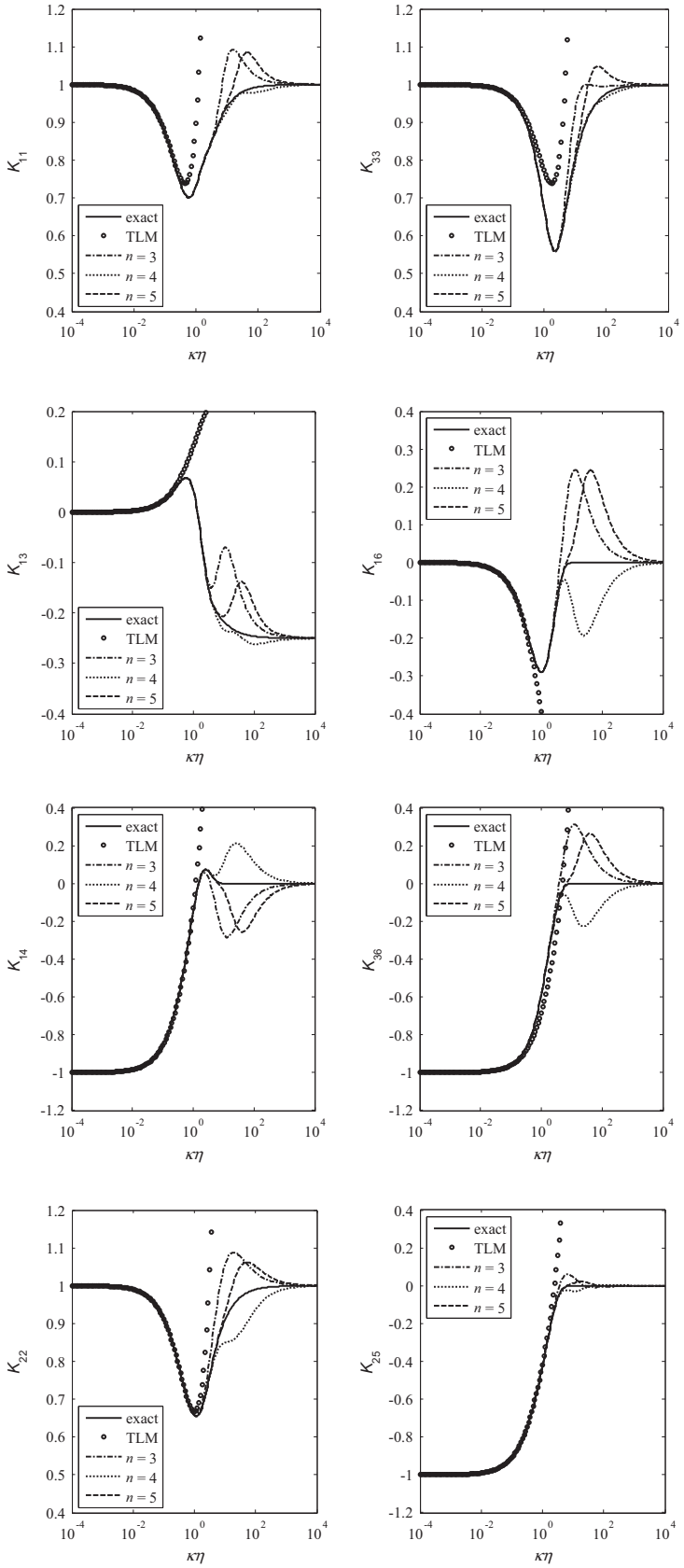

Fig. 2. Approximation of the exact layer stiffness components ($\nu = 1/3$, $\eta < 0.10$).

Table 1
Limiting values of $\kappa\eta$ below which differences between approximate and exact coefficients are less than 1%.

	K_{11}	K_{33}	K_{13}	K_{16}	K_{14}	K_{36}	K_{22}	K_{25}
TLM	0.23	0.23	0.10	0.17	0.24	0.23	0.88	0.84
$n=3$	3.74	3.27	1.14	1.83	1.09	1.52	1.59	1.34
$n=4$	7.06	5.82	3.82	2.91	2.48	2.76	3.85	2.43
$n=5$	9.98	9.14	6.42	4.14	3.96	4.05	7.47	3.64

flexibility coefficients:

$$4\,r\,s-s^4-2\,s^2-1=0 \tag{58}$$

Multiplying by κ^4 and simplifying, the following frequency equation is obtained:

$$4\,\kappa^2\left(\sqrt{\kappa^2-\alpha^2}\sqrt{\kappa^2-1}-\kappa^2+1\right)-1=0 \tag{59}$$

The unbounded amplitude of the half-space flexibility coefficients are related to the Rayleigh waves propagation mode that may be expressed in terms of a single second-order mode, or of two first-order modes:

$$\begin{aligned}\overline{F}_0^{hs} &= \begin{bmatrix}\psi_{\rho,0} & i\,\psi_{\rho,0}\\ \psi_{z,0} & -i\,\psi_{z,0}\end{bmatrix}\begin{bmatrix}\kappa-\kappa_0 & 0\\ 0 & \kappa+\kappa_0\end{bmatrix}^{-1}\begin{bmatrix}\psi_{\rho,0} & \psi_{z,0}\\ i\,\psi_{\rho,0} & -i\,\psi_{z,0}\end{bmatrix}\\ &= \frac{1}{\kappa^2-\kappa_0^2}\begin{bmatrix}\phi_{\rho,0}^2 & \kappa/\kappa_0\times\phi_{\rho,0}\phi_{z,0}\\ \kappa/\kappa_0\times\phi_{\rho,0}\phi_{z,0} & \phi_{z,0}^2\end{bmatrix}\end{aligned} \tag{60}$$

where

$$\phi_{\rho,0}=\sqrt{\sqrt{\kappa_0^2-1}/A_0}\quad \phi_{z,0}=\sqrt{\sqrt{\kappa_0^2-\alpha^2}/A_0} \tag{61}$$

$$\psi_{\rho,0}=\phi_{\rho,0}/\sqrt{2\kappa_0}\quad \psi_{z,0}=\phi_{z,0}/\sqrt{2\,\kappa_0} \tag{62}$$

$$A_0=\frac{8\kappa_0^4-6\kappa_0^2(\alpha^2+1)+4\alpha^2}{\sqrt{\kappa_0^2-\alpha^2}\sqrt{\kappa_0^2-1}}-8\kappa_0^2+4 \tag{63}$$

The "remaining" half-space flexibility matrix is obtained by substracting the contribution of the Rayleigh waves propagation mode from the exact flexibility matrix. The proposed function for adjusting this remaining flexibility matrix consists of a polynomic matrix fraction whose companion matrix form is expressed through first-order eigenvalues:

$$\begin{aligned}\tilde{F}_R^{hs} &= \overline{F}_R^{hs}-\overline{F}_0^{hs}\\ &\approx \left(Q_0+\kappa Q_1+\kappa^2Q_2+\cdots+\kappa^nQ_n+\kappa^{n+1}I\right)^{-1}\left(R_0+\kappa R_1+\kappa^2R_2+\cdots+\kappa^nR_n\right)\end{aligned} \tag{64}$$

This technique was used by Wolf [8] in the frequency domain and in cases of one d.o.f. as is the case for *SH* waves. Matrix R_0 is forced to take the value of the remaining flexibility matrix for $\kappa=0$:

$$R_0=\overline{F}_R^{hs}\Big|_{\kappa=0}-\overline{F}_0^{hs}\Big|_{\kappa=0}=\begin{bmatrix}-i & 0\\ 0 & -i\alpha\end{bmatrix}+\frac{1}{\kappa_0^2}\begin{bmatrix}\phi_{\rho,0}^2 & 0\\ 0 & \phi_{z,0}^2\end{bmatrix} \tag{65}$$

while matrix Q_0 is set as the identity matrix in order to ensure that the approximate flexibility matrix remains exact at $\kappa=0$. Furthermore, matrix R_n is set equal to the remaining flexibility matrix for $\kappa\to\infty$:

$$R_n=\left(\kappa\overline{F}_R^{hs}\right)\Big|_{\kappa\to\infty}-\left(\kappa\overline{F}_0^{hs}\right)\Big|_{\kappa\to\infty}=\frac{1}{2(1-\alpha^2)}\begin{bmatrix}1 & \alpha^2\\ \alpha^2 & 1\end{bmatrix}-\frac{1}{\kappa_0}\begin{bmatrix}0 & \phi_{\rho,0}\phi_{z,0}\\ \phi_{\rho,0}\phi_{z,0} & 0\end{bmatrix} \tag{66}$$

3.2.2. SH waves

Adjustment to the exact half-space flexibility for *SH* waves follows a similar path:

$$\tilde{F}_L^{hs}=\left(Q_0+\kappa Q_1+\kappa^2Q_2+\cdots+\kappa^nQ_n+\kappa^{n+1}I\right)^{-1}\left(R_0+\kappa R_1+\kappa^2R_2+\cdots+\kappa^nR_n\right) \tag{67}$$

Coefficient R_0 takes on the exact value for $\kappa=0$:

$$R_0=\overline{F}_L^{hs}\Big|_{\kappa=0}=-i \tag{68}$$

while coefficient Q_0 is taken as unity. Moreover, the coefficient R_n takes on the exact values of the flexibility for $\kappa\to\infty$:

$$R_n=\left(\kappa\overline{F}_L^{hs}\right)\Big|_{\kappa\to\infty}=1 \tag{69}$$

3.2.3. Adjustment procedure

From Eqs. (64) or (67) one may obtain:

$$\begin{aligned}&\tilde{F}_{R/L}^{hs}+\kappa Q_1\tilde{F}_{R/L}^{hs}+\kappa^2Q_2\tilde{F}_{R/L}^{hs}+\cdots+\kappa^nQ_n\tilde{F}_{R/L}^{hs}+\kappa^{n+1}\tilde{F}_{R/L}^{hs}=R_0+\kappa R_1\\ &\quad+\kappa^2R_2+\cdots+\kappa^nR_n\end{aligned} \tag{70}$$

$$\kappa R_1+\kappa^2R_2+\cdots+\kappa^{n-1}R_{n-1}-\kappa Q_1\tilde{F}_{R/L}^{hs}-\kappa^2Q_2\tilde{F}_{R/L}^{hs}-\cdots-\kappa^nQ_n\tilde{F}_{R/L}^{hs}=\tilde{P} \tag{71}$$

where $\tilde{F}_{R/L}^{hs}$ represents $\tilde{F}_R^{hs}$ or $\tilde{F}_L^{hs}$, and:

$$\tilde{P}=\tilde{F}_{R/L}^{hs}+\kappa^{n+1}\tilde{F}_{R/L}^{hs}-R_0-\kappa^nR_n \tag{72}$$

Adjustment of the approximation coefficients is carried out considering m discrete points for wave number κ. Closeness between these points increases as required by sharp variations in the flexibility coefficients. In this way one arrives at:

$$\tilde{U}\tilde{K}=\tilde{P}\Rightarrow\tilde{U}=\tilde{P}\tilde{K}^{\dagger} \tag{73}$$

where † denotes pseudo-inverse (least squares fit) while:

$$\tilde{U}=\begin{bmatrix}R_1 & R_2 & \cdots & R_{n-1} & Q_1 & Q_2 & \cdots & Q_n\end{bmatrix} \tag{74}$$

$$\tilde{K}=\begin{bmatrix}\kappa_1 I & \kappa_2 I & \cdots & \kappa_m I\\ \kappa_1^2 I & \kappa_2^2 I & \cdots & \kappa_m^2 I\\ \cdots & \cdots & \cdots & \cdots\\ \kappa_1^{n-1} I & \kappa_2^{n-1} I & \cdots & \kappa_m^{n-1} I\\ -\kappa_1\tilde{F}_1 & -\kappa_2\tilde{F}_2 & \cdots & -\kappa_m\tilde{F}_m\\ -\kappa_1^2\tilde{F}_1 & -\kappa_2^2\tilde{F}_2 & \cdots & -\kappa_m^2\tilde{F}_m\\ \cdots & \cdots & \cdots & \cdots\\ -\kappa_1^n\tilde{F}_1 & -\kappa_2^n\tilde{F}_2 & \cdots & -\kappa_m^n\tilde{F}_m\end{bmatrix} \tag{75}$$

$$\tilde{P}=\begin{bmatrix}\tilde{P}_1 & \tilde{P}_2 & \cdots & \tilde{P}_m\end{bmatrix} \tag{76}$$

The companion matrix form associated with the polynomic fraction in (64) or (67) results:

$$\begin{aligned}&\tilde{F}=\tilde{C}\left(\kappa I-\tilde{A}\right)^{-1}\tilde{B}\quad \tilde{C}=\begin{bmatrix}0 & 0 & \cdots & 0 & I\end{bmatrix}\\ &\tilde{B}=\begin{bmatrix}R_0\\ R_1\\ R_2\\ \cdots\\ R_n\end{bmatrix}\qquad \tilde{A}=\begin{bmatrix}0 & 0 & \cdots & 0 & -I\\ I & 0 & \cdots & 0 & -Q_1\\ 0 & I & \cdots & 0 & -Q_2\\ \cdots & \cdots & \cdots & \cdots & \cdots\\ 0 & 0 & \cdots & I & -Q_n\end{bmatrix}\end{aligned} \tag{77}$$

The resolution of the following eigenvalue problem:

$$\tilde{A}\Upsilon=\Upsilon\Lambda \tag{78}$$

allows expressing the half-space flexibility matrix through

first-order modal parameters:

$$\tilde{F} = \Psi_l(\kappa I - \Lambda)^{-1}\Psi_r \tag{79}$$

where

$$\Lambda = \Upsilon^{-1}\tilde{A}\Upsilon \quad \Psi_r = \Upsilon^{-1}\tilde{B} \quad \Psi_l = \tilde{C}\Upsilon \tag{80}$$

In the case of *SV-P* waves, the resulting approximate flexibility matrix in general is non-symmetric so a symmetrization process may be applied to transform the mode shapes matrices by left Ψ_l and by right Ψ_r so that they become the transpose of the other:

$$\Psi_l = \Psi \leftrightarrow \Psi_r = \Psi^T \tag{81}$$

A procedure that allows performing this symmetrization with minimal loss of the accuracy obtained with the polynomial matrix fraction begins with the definition of the following symmetric matrix H_m for each mode m:

$$H_m = 0.5 \times \left(\psi_{l,m}\psi_{r,m} + \psi_{l,m}^T\psi_{r,m}^T\right) \tag{82}$$

This matrix should be singular if the mode shapes by left and by right have the same relationship between their components. The singular value decomposition (SVD) of H_m and the use of the largest singular value leads to a symmetrized mode shape for mode m with a minimal distortion:

$$[U_m, S_m, V_m] = \mathrm{SVD}(H_m) \rightarrow \tilde{H}_m = U_{1:2,1}^m S_{1,1}^m V_{1:2,1}^{m,T} \rightarrow \psi_m = \tilde{H}_{1:2,x}^m / \tilde{H}_{x,x}^m \tag{83}$$

where x represents the index of the component on the main diagonal of $\tilde{H}_m$ with greater absolute value.

A fine-fitting process for the modal parameters may also be applied to compensate for both the linearization effects produced by applying Eq. (71) and an eventual symmetrization process. Techniques to adjust modal parameters, which can be adapted to this case by replacing the exciting frequency with the wave number, and the experimental receptance with the exact flexibility, are presented by Maia and Silva [9].

The proposed iterative fine-fitting process involves six correction factors for each mode: real ($\Re$) and imaginary ($\Im$) parts of the eigenvalue κ_m and the mode shapes components $\psi_{\rho,m}$ and $\psi_{z,m}$. The correction of the components of the remaining half-space flexibility matrix is performed by the following non-dimensional adjustment parameters ("p-values"):

$$\tilde{F}_{\rho\rho}^{corr} = \sum_{m=1}^{M} \frac{\left(\psi_{\rho,m}^{\Re}(1+p_{\rho,m}^{\Re}) + i\psi_{\rho,m}^{\Im}(1+p_{\rho,m}^{\Im})\right)^2}{\kappa - \left(\kappa_m^{\Re}(1+p_{\kappa,m}^{\Re}) + i\kappa_m^{\Im}(1+p_{\kappa,m}^{\Im})\right)} \tag{84}$$

$$\tilde{F}_{zz}^{corr} = \sum_{m=1}^{M} \frac{\left(\psi_{z,m}^{\Re}(1+p_{z,m}^{\Re}) + i\psi_{z,m}^{\Im}(1+p_{z,m}^{\Im})\right)^2}{\kappa - \left(\kappa_m^{\Re}(1+p_{\kappa,m}^{\Re}) + i\kappa_m^{\Im}(1+p_{\kappa,m}^{\Im})\right)} \tag{85}$$

$$\tilde{F}_{\rho z}^{corr} = \sum_{m=1}^{M} \frac{\left(\psi_{\rho,m}^{\Re}(1+p_{\rho,m}^{\Re}) + i\psi_{\rho,m}^{\Im}(1+p_{\rho,m}^{\Im})\right)\left(\psi_{z,m}^{\Re}(1+p_{z,m}^{\Re}) + i\psi_{z,m}^{\Im}(1+p_{z,m}^{\Im})\right)}{\kappa - \left(\kappa_m^{\Re}(1+p_{\kappa,m}^{\Re}) + i\kappa_m^{\Im}(1+p_{\kappa,m}^{\Im})\right)} \tag{86}$$

The linearization of these equations for each wave number κ is performed keeping only the first terms of the partial derivatives shown below:

$$\tilde{F}_{\rho\rho}^{corr} \approx \tilde{F}_{\rho\rho} + \sum_{m=1}^{M}\left(\frac{\partial\tilde{F}_{\rho\rho}}{\partial p_{\kappa,m}^{\Re}}p_{\kappa,m}^{\Re} + \frac{\partial\tilde{F}_{\rho\rho}}{\partial p_{\rho,m}^{\Re}}p_{\rho,m}^{\Re} + \frac{\partial\tilde{F}_{\rho\rho}}{\partial p_{\kappa,m}^{\Im}}p_{\kappa,m}^{\Im} + \frac{\partial\tilde{F}_{\rho\rho}}{\partial p_{\rho,m}^{\Im}}p_{\rho,m}^{\Im}\right) \tag{87}$$

$$\tilde{F}_{zz}^{corr} \approx \tilde{F}_{zz} + \sum_{m=1}^{M}\left(\frac{\partial\tilde{F}_{zz}}{\partial p_{\kappa,m}^{\Re}}p_{\kappa,m}^{\Re} + \frac{\partial\tilde{F}_{zz}}{\partial p_{z,m}^{\Re}}p_{z,m}^{\Re} + \frac{\partial\tilde{F}_{zz}}{\partial p_{\kappa,m}^{\Im}}p_{\kappa,m}^{\Im} + \frac{\partial\tilde{F}_{zz}}{\partial p_{z,m}^{\Im}}p_{z,m}^{\Im}\right) \tag{88}$$

$$\tilde{F}_{\rho z}^{corr} \approx \tilde{F}_{\rho z} + \sum_{m=1}^{M}\begin{pmatrix} \frac{\partial\tilde{F}_{\rho z}}{\partial p_{\kappa,m}^{\Re}}p_{\kappa,m}^{\Re} + \frac{\partial\tilde{F}_{\rho z}}{\partial p_{\rho,m}^{\Re}}p_{\rho,m}^{\Re} + \frac{\partial\tilde{F}_{\rho z}}{\partial p_{z,m}^{\Re}}p_{z,m}^{\Re} + \dots \\ \frac{\partial\tilde{F}_{\rho z}}{\partial p_{\kappa,m}^{\Im}}p_{\kappa,m}^{\Im} + \frac{\partial\tilde{F}_{\rho z}}{\partial p_{\rho,m}^{\Im}}p_{\rho,m}^{\Im} + \frac{\partial\tilde{F}_{\rho z}}{\partial p_{z,m}^{\Im}}p_{z,m}^{\Im} \end{pmatrix} \tag{89}$$

Applying a technique of constrained linear least-squares at each iteration allows limiting the maximum value of p-values to maintain the validity of the linearization and incorporating the appropriate restrictions to maintain the exact values for the doubly-asymptotic condition related with Eqs. (65) and (66). The contribution of the Rayleigh waves propagation mode is finally added to the adjusted modal basis.

Physical matrices of the half-space are obtained by adding auxiliary degrees of freedom in order to accommodate the variation of the flexibility components in the wave number domain as was done for the layers matrices. An alternative to adding the auxiliary degrees of freedom is as follows:

$$\tilde{\Psi} = \begin{bmatrix} \Psi \\ [I \quad 0] \end{bmatrix} \tag{90}$$

where the identity and zero matrices must have the appropriate dimensions so that the extended mode shapes matrix have a square shape. The complete half-space stiffness matrices can then be obtained as:

$$\tilde{K}_A^{hs} = -\tilde{\Psi}^{-T}\Lambda\tilde{\Psi}^{-1} \quad \tilde{K}_B^{hs} = \tilde{\Psi}^{-T}\tilde{\Psi}^{-1} \tag{91}$$

Transforming the auxiliary degrees of freedom, half-space matrices take the following form:

$$K_A^{hs} = \left[\begin{array}{c:c} \hat{K}_0 & 0 \\ \hdashline 0 & I \end{array}\right] \begin{matrix} \} \text{ physical d.o.f.'s} \\ \} \text{ auxiliary d.o.f.'s} \end{matrix} \tag{92}$$

phy. aux.

$$K_B^{hs} = \left[\begin{array}{c:c} \hat{K}_1 & \hat{K}_c^T \\ \hdashline \hat{K}_c & \hat{\Lambda} \end{array}\right] \begin{matrix} \} \text{ physical d.o.f.'s} \\ \} \text{ auxiliary d.o.f.'s} \end{matrix} \tag{93}$$

phy. aux.

The mathematical structure of these matrices is similar to those of the layers, so that their assembly leads to the complete profile matrices. Fig. 3 shows the quality of fit obtained with the described procedure.

3.3. Eigenvalue problem of the soil profile stiffness matrix

The stiffness matrix of the complete soil profile is obained by assembling physical matrices of layers given by Eqs. (27) and (28) with those of the half-space by Eqs. (92) and (93). The contribution to the flexibility of a generic mode m of the second-order approximation (thin-layer method) can be expressed as a combination of two modes of the first-order approach proposed in the present work. These two groups of modes for *SV-P* waves are related by:

$$\tilde{F}_m = \begin{bmatrix} \psi_{\rho,m} & i\,\psi_{\rho,m} \\ \psi_{z,m} & -i\,\psi_{z,m} \end{bmatrix}\begin{bmatrix} \kappa-\kappa_m & 0 \\ 0 & \kappa+\kappa_m \end{bmatrix}^{-1}\begin{bmatrix} \psi_{\rho,m} & \psi_{z,m} \\ i\,\psi_{\rho,m} & -i\,\psi_{z,m} \end{bmatrix}$$

$$
\begin{aligned}
&= \frac{1}{\kappa-\kappa_m}\begin{bmatrix} \psi_{\rho,m}^2 & \psi_{\rho,m}\psi_{z,m} \\ \psi_{z,m}\psi_{\rho,m} & \psi_{z,m}^2 \end{bmatrix} + \frac{1}{\kappa+\kappa_m}\begin{bmatrix} -\psi_{\rho,m}^2 & \psi_{\rho,m}\psi_{z,m} \\ \psi_{z,m}\psi_{\rho,m} & -\psi_{z,m}^2 \end{bmatrix} \\
&= \frac{1}{\kappa^2-\kappa_m^2}\left((\kappa+\kappa_m)\begin{bmatrix} \psi_{\rho,m}^2 & \psi_{\rho,m}\psi_{z,m} \\ \psi_{z,m}\psi_{\rho,m} & \psi_{z,m}^2 \end{bmatrix} \right. \\
&\quad \left. +(\kappa-\kappa_m)\begin{bmatrix} -\psi_{\rho,m}^2 & \psi_{\rho,m}\psi_{z,m} \\ \psi_{z,m}\psi_{\rho,m} & -\psi_{z,m}^2 \end{bmatrix} \right) \\
&= \frac{2\kappa_m}{\kappa^2-\kappa_m^2}\begin{bmatrix} \psi_{\rho,m}^2 & \kappa/\kappa_m \times \psi_{\rho,m}\psi_{z,m} \\ \kappa/\kappa_m \times \psi_{z,m}\psi_{\rho,m} & \psi_{z,m}^2 \end{bmatrix} \\
&= \frac{1}{\kappa^2-\kappa_m^2}\begin{bmatrix} \phi_{\rho,m}^2 & \kappa/\kappa_m \times \phi_{\rho,m}\phi_{z,m} \\ \kappa/\kappa_m \times \phi_{z,m}\phi_{\rho,m} & \phi_{z,m}^2 \end{bmatrix}
\end{aligned} \tag{94}
$$

where

$$
\begin{aligned}
\phi_{\rho,m} &= \sqrt{2\kappa_m} \times \psi_{\rho,m} \\
\phi_{z,m} &= \sqrt{2\kappa_m} \times \psi_{z,m}
\end{aligned} \tag{95}
$$

This relationship between first and second-order modes is identical to that of the Rayleigh waves propagation mode given by Eq. (60).

A particular feature of the first-order approximation is that the eigenvalues of the soil profile appear in the four quadrants of the complex plane, unlike the second-order approximation where it is possible to "choose" the eigenvalues with non-positive imaginary part (3rd and 4th quadrants). However, the contribution to the spatial response of the second-order mode in Eq. (94) is identical to the combination of the two first-order associated modes, expressing the contribution of the mode with eigenvalues with non-positive imaginary part through a Hankel function of second kind, and that of the mode with eigenvalue with positive imaginary part through a Hankel function of first kind, as shown in [10].

Another characteristic of the approach proposed here is that not all modes have an associate mode with an eigenvalue with the opposite sign. These single modes are required to reproduce the exact coefficients for $\kappa \to \infty$, and to achieve the capacity to adequately represent the static response of the soil profile.

Note that material hysteretic damping β may be introduced through the eigenvalues:

$$
\kappa_m^* = \frac{\kappa_m}{(1+i\beta_m)} \tag{96}
$$

The relationship between dimensional and non-dimensional modal parameters is:

$$
s_m = \frac{\omega}{V_S}\kappa_m \quad \varphi_m = \frac{1}{\sqrt{\bar{\rho}}\,V_S}\psi_m \tag{97}
$$

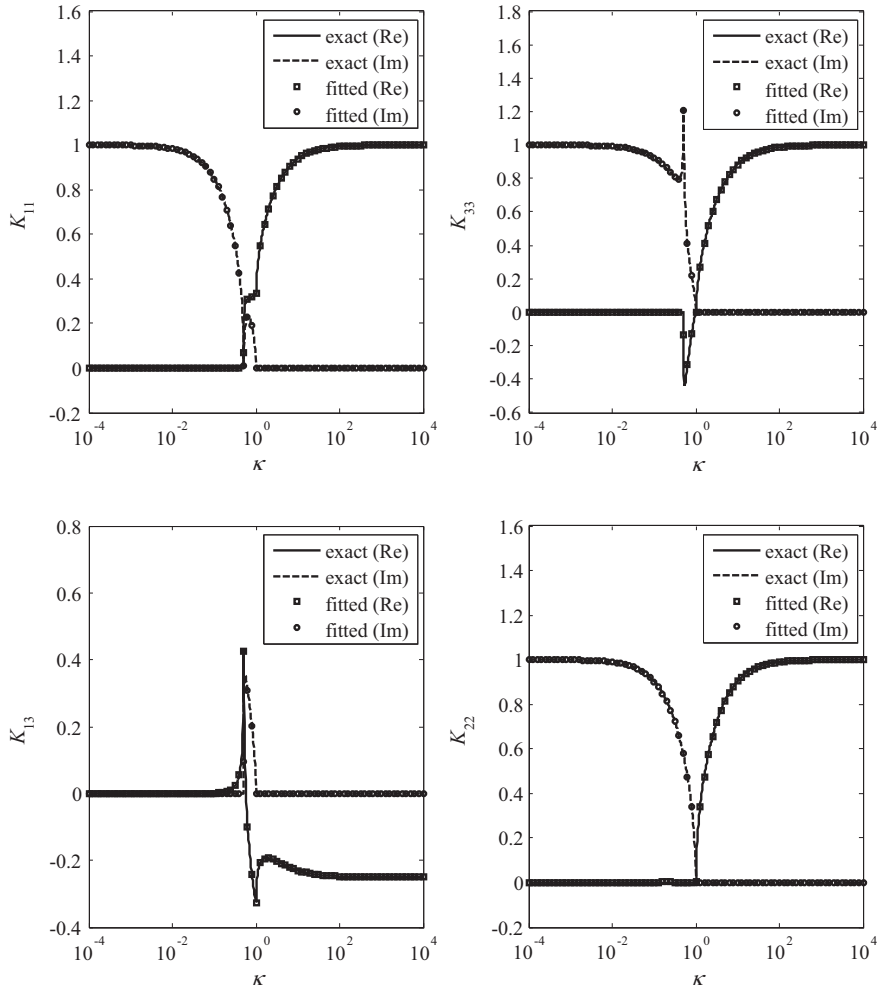

Fig. 3. Approximation of the exact components of the half-space stiffness ($\nu = 1/3$).

The soil profile flexibility given by Eq. (8) at the jth interface results:

$$F(k)_j = \begin{bmatrix} \sum_{m=1}^{M} \frac{\varphi_{\rho,m}^2}{k-s_m} & 0 & \sum_{m=1}^{M} \frac{\varphi_{\rho,m}\,\varphi_{z,m}}{k-s_m} \\ 0 & \sum_{n=1}^{N} \frac{\varphi_{\theta,n}^2}{k-s_n} & 0 \\ \sum_{m=1}^{M} \frac{\varphi_{z,m}\,\varphi_{\rho,m}}{k-s_m} & 0 & \sum_{m=1}^{M} \frac{\varphi_{z,m}^2}{k-s_m} \end{bmatrix} \tag{98}$$

while for the static case this flexibility is:

$$F(k)_j\big|_{\omega=0} = \frac{1}{k} \begin{bmatrix} \sum_{m=1}^{M} \varphi_{\rho,m}^2 & 0 & \sum_{m=1}^{M} \varphi_{\rho,m}\,\varphi_{z,m} \\ 0 & \sum_{n=1}^{N} \varphi_{\theta,n}^2 & 0 \\ \sum_{m=1}^{M} \varphi_{z,m}\,\varphi_{\rho,m} & 0 & \sum_{m=1}^{M} \varphi_{z,m}^2 \end{bmatrix} \tag{99}$$

4. Spatial response for three-dimensional problems

The capacity of the proposed formulation to describe the response of a soil profile to different loads is analyzed through comparisons with known exact solutions (see Kausel [11]) and numerical solutions obtained with a commercial program based on the thin-layer method.

4.1. Point loads

The first kind of analyzed cases is that of harmonic point loads at the surface of different soil profiles. For a vertical point load, matrices C and T of Eqs. (3) and (4) take on the form ($\mu=0$):

$$C = \begin{bmatrix} -J_1(k\rho) & 0 & 0 \\ 0 & -J_1(k\rho) & 0 \\ 0 & 0 & -J_0(k\rho) \end{bmatrix} \quad T = \begin{bmatrix} 1 & 0 & 0 \\ 0 & 0 & 0 \\ 0 & 0 & 1 \end{bmatrix} \tag{100}$$

The transformation of the corresponding load to the wave number domain leads to:

$$P_1 = \frac{\delta(\rho)}{\rho} \begin{bmatrix} 0 \\ 0 \\ 1 \end{bmatrix} \leftrightarrow \overline{P}_1 = -\frac{1}{2\pi} \begin{bmatrix} 0 \\ 0 \\ 1 \end{bmatrix} \tag{101}$$

where $\delta(\rho)$ is the Dirac delta function. The static displacements at the surface according to (99) are:

$$\overline{U}_1 = -\frac{1}{2\pi}\frac{1}{k} \begin{bmatrix} \sum_{m=1}^{M} \varphi_{\rho,m}\varphi_{z,m} \\ 0 \\ \sum_{m=1}^{M} \varphi_{z,m}^2 \end{bmatrix} \leftrightarrow U_1 = \frac{1}{2\pi} \begin{bmatrix} \int_0^\infty J_1(k\rho)dk \times \sum_{m=1}^{M} \varphi_{\rho,m}\,\varphi_{z,m} \\ 0 \\ \int_0^\infty J_0(k\rho)dk \times \sum_{m=1}^{M} \varphi_{z,m}^2 \end{bmatrix} \tag{102}$$

Therefore, the vertical displacement at the surface is:

$$U_{z,1} = \frac{1}{2\pi}\frac{1}{\rho} \sum_{m=1}^{M} \varphi_{z,m}^2 \tag{103}$$

According to the restriction imposed by Eq. (66) for a homogeneous half-space, the summation term in (103) is:

$$\sum_{m=1}^{M} \varphi_{z,m}^2 = \frac{1}{2(1-\alpha^2)}\frac{1}{\overline{\rho} V_S^2} \tag{104}$$

and therefore:

$$U_{z,1} = \frac{1}{4\pi(1-\alpha^2)}\frac{1}{\overline{\rho} V_S^2}\frac{1}{\rho} \tag{105}$$

This result is also found in classic books of elastodynamics such as Ewing et al. [12].

The dynamic displacements at the surface according to (98) are given by:

$$\overline{U} = -\frac{1}{2\pi} \begin{bmatrix} \sum_{m=1}^{M} \frac{\varphi_{\rho,m}\,\varphi_{z,m}}{k-s_m} \\ 0 \\ \sum_{m=1}^{M} \frac{\varphi_{z,m}^2}{k-s_m} \end{bmatrix} \leftrightarrow U = \frac{1}{2\pi} \begin{bmatrix} U_{\rho z}(\rho) \\ 0 \\ U_{zz}(\rho) \end{bmatrix} \tag{106}$$

$$U_{\rho z}(\rho) = \sum_{m=1}^{M} \varphi_{\rho,m}\varphi_{z,m} \int_0^\infty \frac{kJ_1(k\rho)}{k-s_m}dk \tag{107}$$

$$U_{zz}(\rho) = \sum_{m=1}^{M} \varphi_{z,m}^2 \int_0^\infty \frac{kJ_0(k\rho)}{k-s_m}dk \tag{108}$$

Integrals in (107) and (108) for $Re(s_m) \le 0$ are:

$$\begin{cases} \int_0^\infty \frac{kJ_1(k\rho)}{k-s_m}dk = s_m\left(1-\frac{\pi}{2}\left(\boldsymbol{H}_1(-s_m\rho)-Y_1(-s_m\rho)\right)\right) \\ \int_0^\infty \frac{kJ_0(k\rho)}{k-s_m}dk = \frac{1}{\rho}+\frac{\pi s_m}{2}\left(\boldsymbol{H}_0(-s_m\rho)-Y_0(-s_m\rho)\right) \end{cases} \tag{109}$$

while for $Re(s_m) > 0$, starting from Eq. (94), they are found to be:

$$\begin{cases} \int_0^\infty \frac{kJ_1(k\rho)}{k-s_m}dk = 2\int_0^\infty \frac{k^2J_1(k\rho)}{k^2-s_m^2}dk - \int_0^\infty \frac{kJ_1(k\rho)}{k+s_m}dk = (-1)^{q-1}i\pi s_m H_1^{(q)}(s_m\rho)+s_m\left(1-\frac{\pi}{2}\left(\boldsymbol{H}_1(s_m\rho)-Y_1(s_m\rho)\right)\right) \\ \int_0^\infty \frac{kJ_0(k\rho)}{k-s_m}dk = 2s_m\int_0^\infty \frac{kJ_0(k\rho)}{k^2-s_m^2}dk + \int_0^\infty \frac{kJ_0(k\rho)}{k+s_m}dk = (-1)^{q-1}i\pi s_m H_0^{(q)}(s_m\rho)+\frac{1}{\rho}-\frac{\pi s_m}{2}\left(\boldsymbol{H}_0(s_m\rho)-Y_0(s_m\rho)\right) \end{cases} \tag{110}$$

where $q=1$ is for eigenvalues in the first quadrant, and $q=2$ is for the fourth quadrant including the positive real axis.

In the case of a horizontal point load, matrices C and T in Eqs. (3) and (4) take on the form ($\mu=1$):

$$C = \begin{bmatrix} J_0(k\rho)-J_1(k\rho)/(k\rho) & J_1(k\rho)/(k\rho) & 0 \\ J_1(k\rho)/(k\rho) & J_0(k\rho)-J_1(k\rho)/(k\rho) & 0 \\ 0 & 0 & -J_1(k\rho) \end{bmatrix}$$

$$T = \begin{bmatrix} \cos(\theta) & 0 & 0 \\ 0 & -\sin(\theta) & 0 \\ 0 & 0 & \cos(\theta) \end{bmatrix} \tag{111}$$

The transformation of the corresponding load to the wave number domain leads to:

$$P = \frac{\delta(\rho)}{2\pi\rho} \begin{bmatrix} \cos(\theta) \\ -\sin(\theta) \\ 0 \end{bmatrix} \leftrightarrow \overline{P} = \frac{1}{2\pi} \begin{bmatrix} 1 \\ 1 \\ 0 \end{bmatrix} \tag{112}$$

The dynamic displacements at the surface are calculated as:

$$\overline{U}=\frac{1}{2\pi}\begin{bmatrix}\sum_{m=1}^{M}\frac{\phi_{\rho,m}^2}{k-s_m}\\ \sum_{n=1}^{N}\frac{\phi_{\theta,n}^2}{k-s_n}\\ \sum_{m=1}^{M}\frac{\phi_{z,m}\phi_{\rho,m}}{k-s_m}\end{bmatrix}\leftrightarrow U=\frac{1}{2\pi}\begin{bmatrix}U_{\rho x}(\rho)\times\cos(\theta)\\ U_{\theta x}(\rho)\times\sin(\theta)\\ U_{zx}(\rho)\times\cos(\theta)\end{bmatrix} \tag{113}$$

$$U_{\rho x}(\rho)=\sum_{m=1}^{M}\phi_{\rho,m}^2\left(\int_0^\infty\frac{kJ_0(k\rho)}{k-s_m}dk-\frac{1}{\rho}\int_0^\infty\frac{J_1(k\rho)}{k-s_m}dk\right)+\sum_{n=1}^{N}\phi_{\theta,n}^2\frac{1}{\rho}\int_0^\infty\frac{J_1(k\rho)}{k-s_n}dk \tag{114}$$

$$U_{\theta x}(\rho)=\sum_{n=1}^{N}\phi_{\theta,n}^2\left(\frac{1}{\rho}\int_0^\infty\frac{J_1(k\rho)}{k-s_n}dk-\int_0^\infty\frac{kJ_0(k\rho)}{k-s_n}dk\right)-\sum_{m=1}^{M}\phi_{\rho,m}^2\frac{1}{\rho}\int_0^\infty\frac{J_1(k\rho)}{k-s_m}dk \tag{115}$$

$$U_{zx}(\rho)=-\sum_{m=1}^{M}\phi_{z,m}\phi_{\rho,m}\int_0^\infty\frac{kJ_1(k\rho)}{k-s_m}dk \tag{116}$$

Comparing (107) with (116) if follows that:

$$U_{zx}(\rho)=-U_{\rho z}(\rho) \tag{117}$$

The integral in (114) and (115) that does not appear in (109) is for $Re(s_m)\le 0$ given by:

$$\int_0^\infty\frac{J_1(k\rho)}{k-s_m}dk=1-\frac{\pi}{2}(\boldsymbol{H}_1(-s_m\rho)-Y_1(-s_m\rho))-\frac{1}{s_m\rho} \tag{118}$$

while, after manipuating Eq. (94), it is for $Re(s_m)>0$ given by:

$$\begin{aligned}\int_0^\infty\frac{J_1(k\rho)}{k-s_m}dk&=2\,s_m\int_0^\infty\frac{J_1(k\rho)}{k^2-s_m^2}dk+\int_0^\infty\frac{J_1(k\rho)}{k+s_m}dk\\&=(-1)^{q-1}i\pi H_1^{(q)}(s_m\rho)+1-\frac{\pi}{2}(\boldsymbol{H}_1(s_m\rho)-Y_1(s_m\rho))-\frac{1}{s_m\rho}\end{aligned} \tag{119}$$

where $q=1$ applies for eigenvalues in the first quadrant, and $q=2$ for those in the fourth quadrant including the positive real axis.

To evaluate the accuracy of the approximation for the half-space, Figs. 4 and 5 show the response at the surface of a homogenous half-space for $\nu=1/3$ obtained for a vertical and horizontal point load, respectively. Displacements and radial coordinates are non-dimensionalized as:

$$u=2\pi\frac{\overline{\rho}\,V_S^3}{\omega}U;\rho_0=\frac{\omega}{V_S}\rho \tag{120}$$

The accuracy of the approximation obtained for the layers is shown through the response at the surface of a layer supported on a rigid half-space. Fig. 6 corresponds to the case of a layer with non-dimensional thickness $\eta=0.49\pi$ for which the dynamic flexibility coefficients do not present singularities and the imaginary part of the displacements is null. The nature of response changes starting form $\eta=\pi/2$ when the layer begins to dissipate energy by radiation. Fig. 7 corresponds to the case of a layer with thickness $\eta=1.01\pi$, where the dynamic flexibility coefficients present two singularities associated with surface waves propagation modes.

The exact solutions for point loads were obtained from the exact matrices given in (11), (21) and (23). The singularities of the flexibility coefficients are eliminated substracting the modes with real eigenvalues obtained with FODAP. These modes are then analytically transformed to the space domail, while the remaining flexibility by numerical integration from $\kappa=0$ to $\kappa=50$, the latter being the value of κ for which are sufficiently closed to their assymptotic values, and analitically from $\kappa=50$ up to infinity. The flexibility coefficient $\overline{K}_L^{ns}$ may be analytically transformed without difficulty to the space domain. It may be observed that the approximation obtained for both analyzed profiles turns out excellent.

4.2. Disk loads

The second kind of cases analyzed here corresponds to harmonic distributed loads applied at a circular area on the surface of different soil profiles. For vertical loads, matrices C and T are identical to those of Eq. (100). The load vector in this case is:

$$P_1=\begin{bmatrix}0\\0\\1\end{bmatrix}\quad\leftrightarrow\quad\overline{P}_1=-\frac{R}{k}J_1(kR)\begin{bmatrix}0\\0\\1\end{bmatrix} \tag{121}$$

where R is the radius of the disc (circular area). The static displacement vector at the surface results:

$$\overline{U}_1=-\frac{R}{k^2}J_1(kR)\begin{bmatrix}\sum_{m=1}^{M}\varphi_{\rho,m}\,\varphi_{z,m}\\0\\\sum_{m=1}^{M}\varphi_{z,m}^2\end{bmatrix}\leftrightarrow U_1=\begin{bmatrix}R\int_0^\infty\frac{J_1(k\rho)J_1(kR)}{k}dk\times\sum_{m=1}^{M}\varphi_{\rho,m}\,\varphi_{z,m}\\0\\R\int_0^\infty\frac{J_0(k\rho)J_1(kR)}{k}dk\times\sum_{m=1}^{M}\varphi_{z,m}^2\end{bmatrix} \tag{122}$$

Thus, the vertical displacement at the surface is:

$$U_{z,1}=\begin{cases}\frac{2R}{\pi}E(\rho/R)\sum_{m=1}^{M}\varphi_{z,m}^2 & \rho\le R\\ \frac{2\rho}{\pi}\left(E(R/\rho)-\left(1-(R/\rho)^2\right)K(R/\rho)\right)\sum_{m=1}^{M}\varphi_{z,m}^2 & \rho\ge R\end{cases} \tag{123}$$

where E and K are functions known as complete elliptic integrals (for example, see [13]). Note that the expression for $\rho\ge R$ in Eq. (123) takes the form of Eq. (105) dividing by the disk area and taking limit for $R\to 0$.

The general form of the Hankel transform to calculate the contribution of a generic mode of eigenvalue s to the dynamic displacements in cylindrical coordinates is:

$$V_{\alpha\beta\gamma}(\rho,R,s)=\int_0^\infty\frac{J_\beta(k\rho)J_\gamma(kR)}{k^\alpha(k-s)}dk \tag{124}$$

Response along coordinate ρ has a non-oscillating nature when the real part of s is negative (2nd and 3rd quadrants). In this case, the integrand has no unbounded values and the integrals are solved numerically with good accuracy through series expansions as shown by Hemsley [14]. The numerical solutions are based on substitutions of the type:

$$\begin{aligned}J_0(k\rho)J_0(kR)&=\tfrac{1}{\pi}\textstyle\int_0^\pi J_0(k\overline{r})d\theta\\ J_1(k\rho)J_1(kR)&=\frac{k\rho R}{\pi}\int_0^\pi J_1(k\overline{r})\frac{\sin^2\theta}{\overline{r}}d\theta\end{aligned} \tag{125}$$

where

$$\overline{r}=\sqrt{\rho^2+R^2-2\rho R\,\cos\,\theta} \tag{126}$$

The more complex integrals of (124) may be expressed in terms of simpler integrals such as:

$$V_{001}(\rho,R,s)=\tfrac{1}{\rho}V_{111}(\rho,R,s)+\tfrac{\partial}{\partial\rho}V_{111}(\rho,R,s)$$

$$V_{010}(\rho,R,s)=\frac{1}{R}V_{111}(\rho,R,s)+\frac{\partial}{\partial R}V_{111}(\rho,R,s) \tag{127}$$

The nature of the reponse is oscillating along coordinate ρ when the real part of s is positive (1st and 4th quadrants), and the integrals are handled as follows. According to (94), the terms related with the main diagonal of the flexibility matrix (direct terms) are calculated as:

$$V_{\alpha\beta\gamma}(\rho,R,s)=2s\int_0^\infty \frac{J_\beta(k\rho)J_\gamma(kR)}{k^\alpha(k^2-s^2)}dk+\int_0^\infty \frac{J_\beta(k\rho)J_\gamma(kR)}{k^\alpha(k+s)}dk \tag{128}$$

while the terms related with the coefficients outside the main

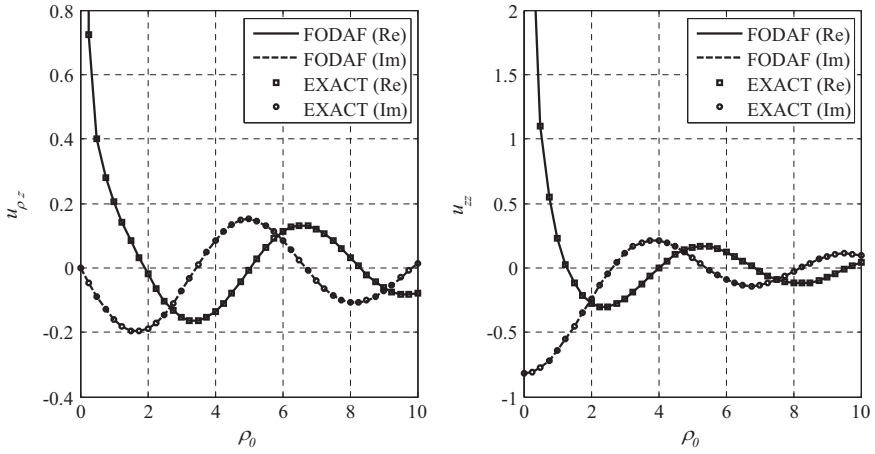

Fig. 4. Displacements at surface of a half-space due to a harmonic vertical point load.

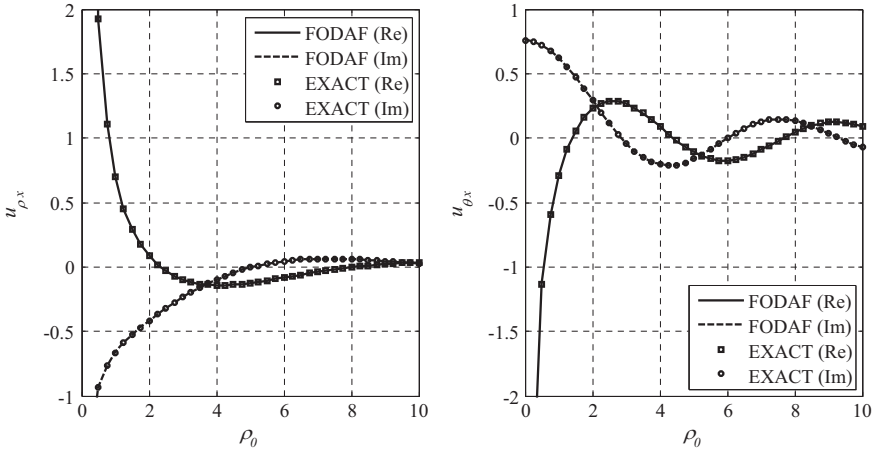

Fig. 5. Displacements at surface of a half-space due to a harmonic horizontal point load.

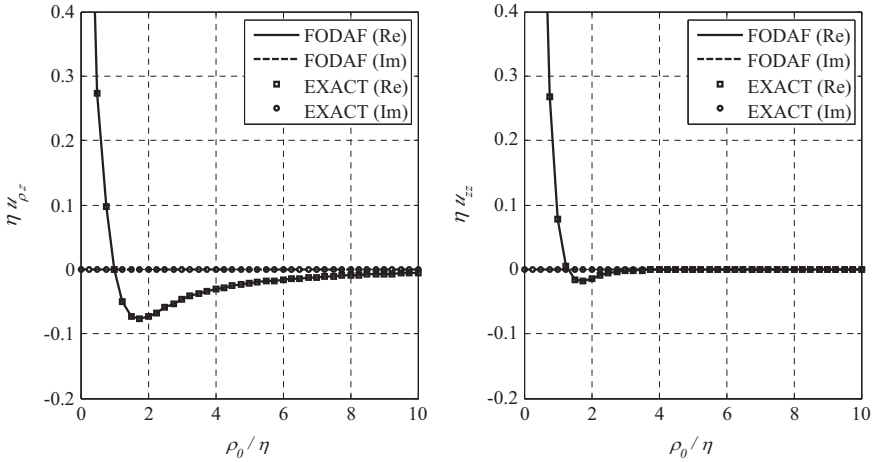

Fig. 6. Displacements at surface of a layer due to a vertical point load ($\eta=0.49\pi$).

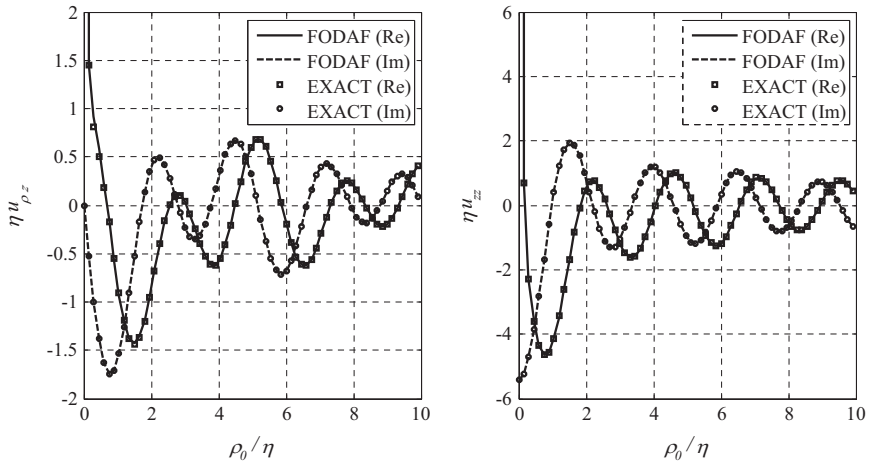

Fig. 7. Displacements at surface of a layer due to a vertical point load ($\eta = 1.01\pi$).

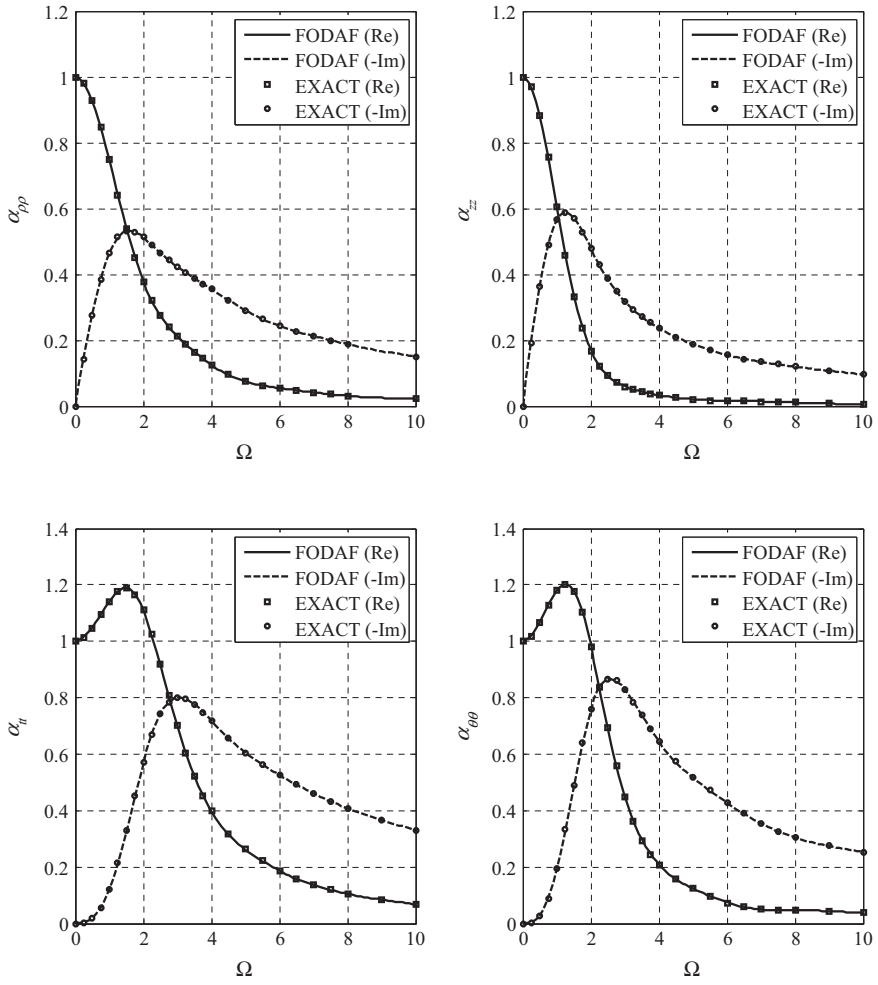

Fig. 8. Dynamic flexibility components of a rigid disc with relaxed boundary conditions.

diagonal of the flexibility matrix (cross terms) are obtained through:

$$V_{\alpha\beta\gamma}(\rho,R,s) = 2\int_0^\infty \frac{J_\beta(k\rho)J_\gamma(kR)}{k^{\alpha-1}(k^2-s^2)}dk - \int_0^\infty \frac{J_\beta(k\rho)J_\gamma(kR)}{k^\alpha(k+s)}dk \qquad (129)$$

First terms of Eqs. (128) and (129) are solved analytically, while second terms are computed numerically as performed for 2nd and 3rd quadrants. The oscillating part of these integrals is due to the first terms, which are identical to those arising from the second-order approach (see Kausel [15] for the solution of some of these integrals).

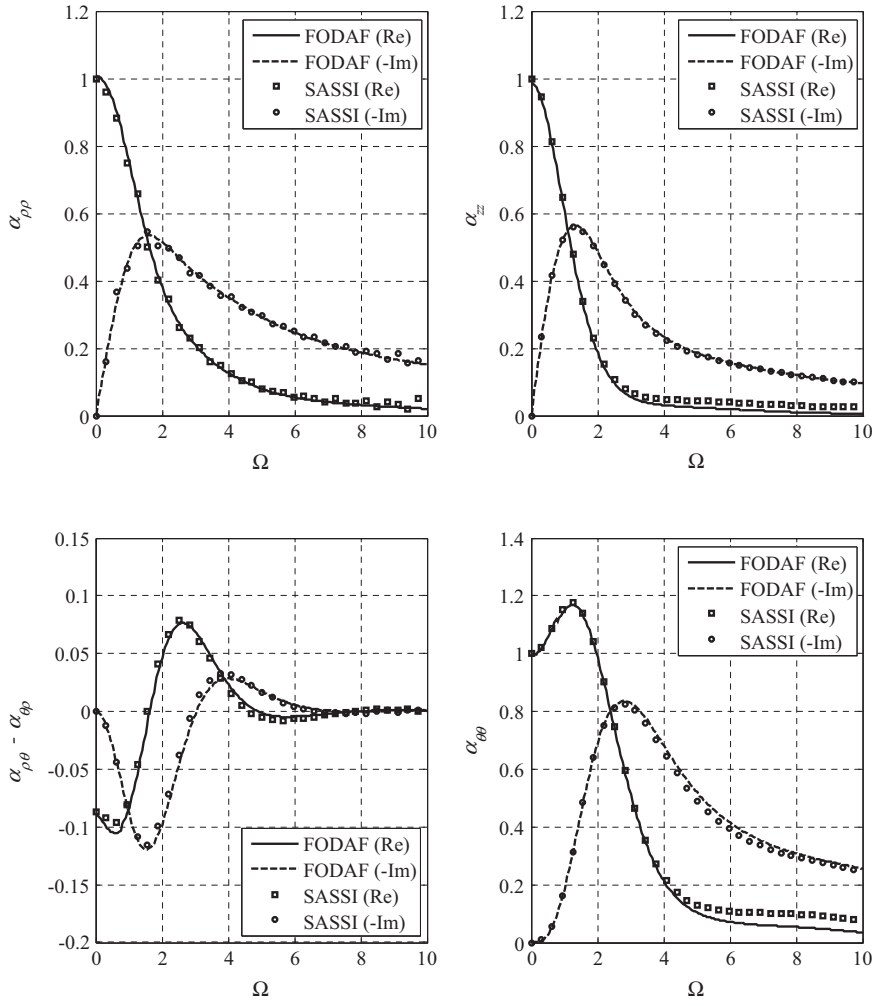

Fig. 9. Dynamic flexibility components for Case 1.

The flexibility of the rigid circular plates resting on different soil profiles is calculated by inversion of the stiffness matrix obtained with the ring method ([16]). Reponse for each anular load is obtained as the difference between that of two disks of different diameter subject to uniform load of different sign. Since the stresses have a singularity at the disk edges, the ring widths are gradually reduced near the edges to smoothen the effect of such unbounded value. In the analyzed cases, 50 rings are used. The excitation frequency is defined as:

$$\Omega = \frac{R}{V_S} \times \omega \tag{130}$$

where V_S is the shear wave velocity at the free surface. All cases are for $\nu = 1/3$.

In the first analysed cases, relaxed boundary conditions are assumed for the compatibility conditions at the center of the rings, thus allowing a comparison of results between the proposed formulation to the exact ones presented by Luco and Westman [17]. Some valuable details associated with the numerical evaluation of these curves were present by Veletsos and Wei [18], and Wei [19]. In fact, to obatin the flexibility component $\alpha_{\rho\rho}$ it is required a special treatment for the numerical integration of functions with singularities and discontinuities, so have been taken for this case the values tabulated in these last works. Fig. 8 shows the excellent agreement between the exact solutions and those provided by FODAF.

At this point it is considered worthwhile to remark some difficulties of the TLM to adequately represent the elastic half-space. With this aim, the dynamic flexibility of disks obtained with the commercial program SASSI [20], which is based precisely on the TLM, are presented in what follows, assuming welded contact for the compatibility conditions at the center of the rings.

Three different cases are analyzed: (1) homogeneous half-space, (2) homogeneous stratum of thickness equal to the disk diameter, resting on a rigid half-space, and (3) same as Case 2 but with an elastic half-space of shear wave velocity equal to 2.5 times that of the stratum.

Figs. 9–11 present a comparison of the flexibility curves, where non-dimensional form is adopted with reference to the static flexibility of Case 1. In general, very good agreement is obtained for all cases. The $\alpha_{\rho\rho}$ component in Case 1 for the homogeneous half-space presents oscillations about values obtained with FODAF. Components α_{zz} and $\alpha_{\theta\theta}$ show for high frequencies differences in the real part that reach up to a factor of about 2. Nevertheless, these differences are much smaller when the comparison is drawn on the basis of the modulus of the flexibility due to the influence of the imaginary part in those frequencies. It is worth pointing out that no radiation damping is found in Case 2 for frequencies below the fundamental frequency of the stratum, as represented by zero imaginary part of $\alpha_{\rho\rho}$ for frequencies below $\Omega = \pi/4$, and less rigorously for α_{zz} and $\alpha_{\theta\theta}$ for frequencies below $\Omega = \pi/2$.

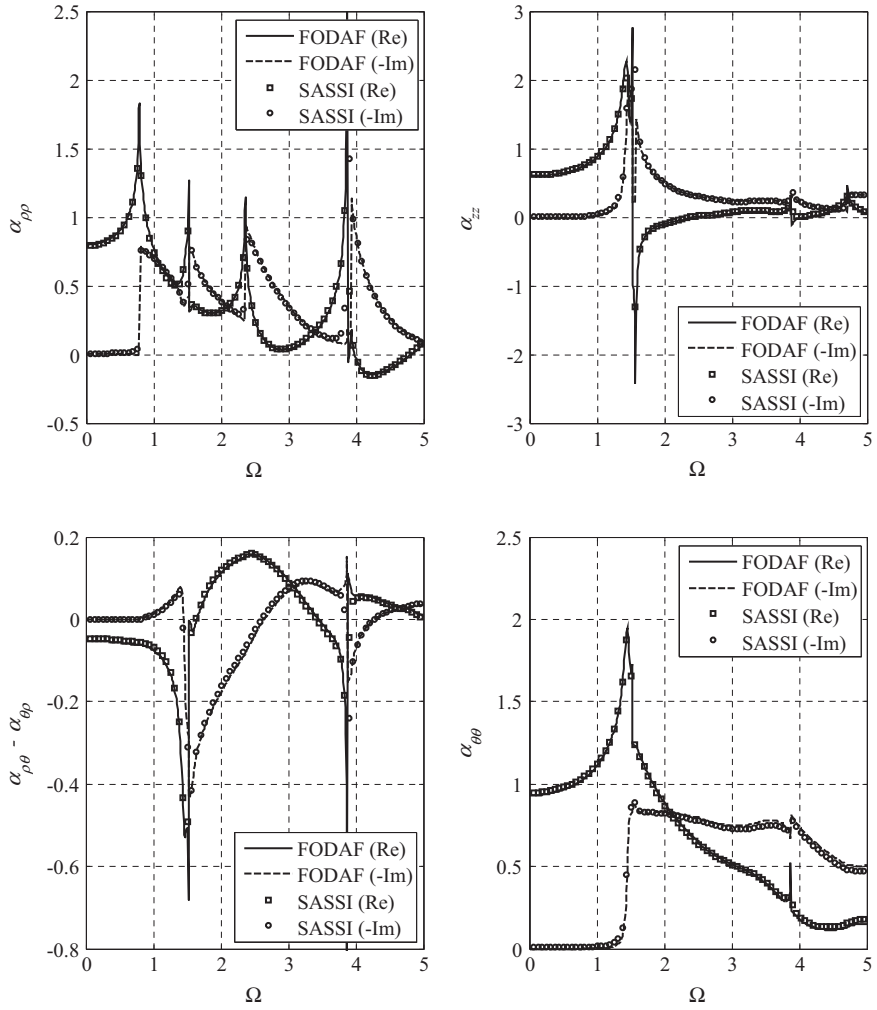

Fig. 10. Dynamic flexibility components for Case 2.

Of particular interest is the location of the soil profile eigenvalues in the complex plane for different excitation frequencies. Fig. 12 shows the eigenvalues for Case 3 for *SV-P* waves and excitation frequencies in the range 0–5 with increments of 0.25. The left part of Fig. 12 shows the general pattern of eigenvalues, while the right part is a blow-up of the same graphic near the origin. First quadrant eigenvalues corresponding to oscillating modes are relatively few and are far from the positive real axis, so that the corresponding modes attenuate quickly away from the source in the spatial domain. Eigenvalues on the positive real axis should be considered belonging to the 4th quadrant and correspond to oscillating modes that attenuate only due to radiation damping. The correct separation between eigenvalues of the 1st and 4th quadrant is mandatory due to abrupt changes in the solution of integrals (128) and (129). This effect is due to the real part of these solutions is symmetric about the real axis, while the imaginary part is anti-symmetric taking on non-zero values near the positive real axis. The approximation of the half-space stiffness may generate small numerical inaccuracies that send some eigenvalues from the positive real axis to the first quadrant, therefore it is necessary to eliminate the imaginary part of these eigenvalues to force them to contribute to the correct solution. The observations made above about this case are representative of what happens in the other cases.

5. Conclusions

An approximate formulation to the direct stiffness method has been presented that provides an alternative to the thin-layer method using first-order modal parameters instead of second-order ones, and in so doing results doubly-asymptotic in nature since it tends to the exact solution for wave numbers tending both to zero and to infinity. In this formulation, as in the exact solution, the stiffness coefficients of the underlying half-space are complex retaining the capacity to represent radiation damping without the need to consider artificial additional terms. The proposed formulation is more accurate as compared to previously available alternatives, and also allows obtaining the static solution as a particular case.

Exact solutions and rigid disk examples resting on typical soil profiles illustrate excellent capacity to represent the known exact solution cases, suggesting the potential of this formulation for application in other more complex elastodynamic problems. Other potential applications of the proposed approach are: (a) site characterization by wave propagation methods, (b) wave amplification through layered media, (c) determination of the dynamic stiffness of rigid foundations for a wide range of frequencies, and (d) study of dynamic soil–structure interaction problems.

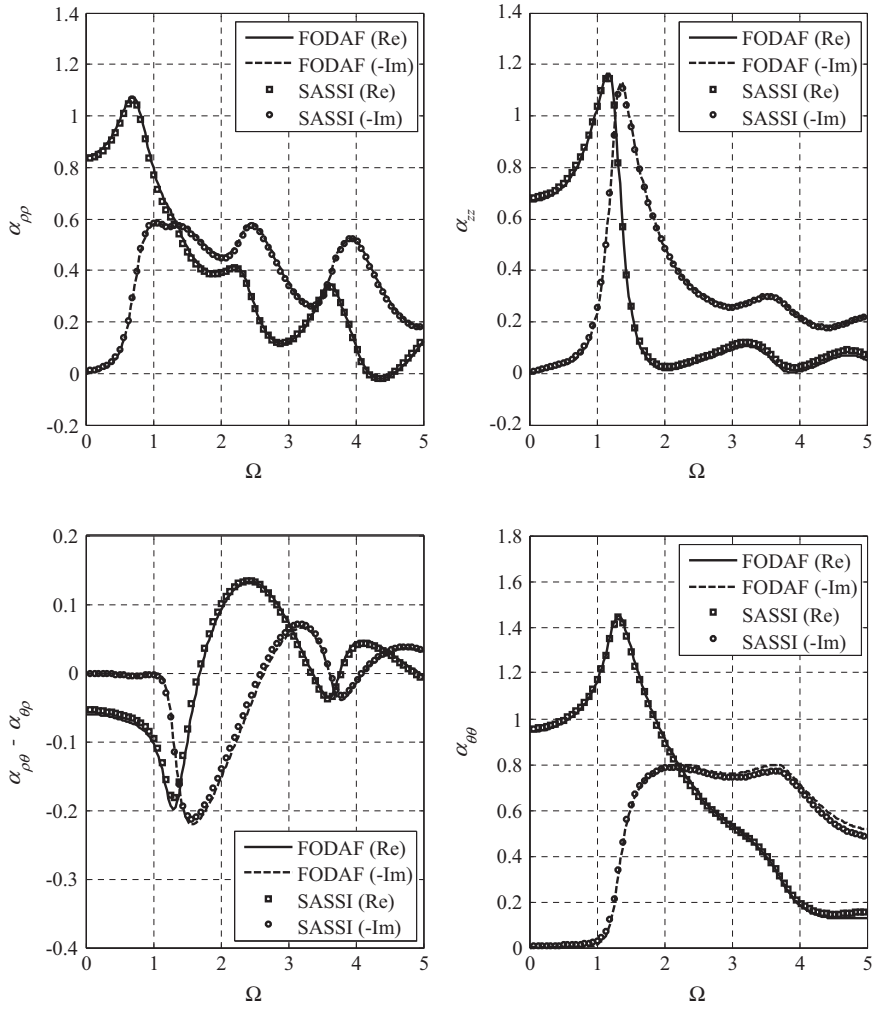

Fig. 11. Dynamic flexibility components for Case 3.

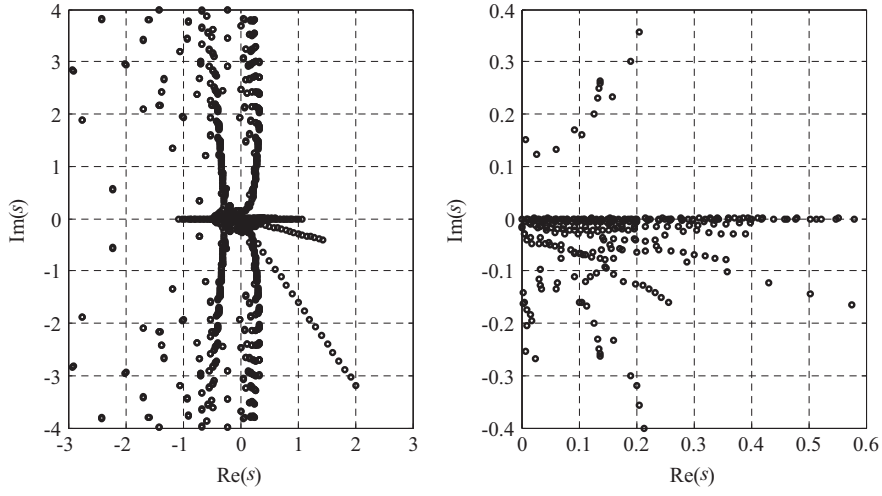

Fig. 12. Distribution of eigenvalues in the complex plane for Case 3.

Acknowledgements

The present work was partially supported by the Consejo Nacional de Investigaciones Científicas y Técnicas (CONICET) and the Secretaría de Ciencia y Tecnología, Universidad Nacional de Córdoba, Argentina. Longstanding support of these institutions over a number of years is greatly appreciated by the authors.

References

[1] Kausel E, Roesset JM. Stiffness matrices for layered soils. Bull Seismol Soc Am 1981;71(6):1743–61.
[2] Kausel E. An explicit solution for the Green functions for dynamic loads in layered media. MIT research report R81-13. Department of Civil Engineering, Cambridge; 1981.
[3] Park J. Wave motion in finite and infinite media using the Thin-Layer Method. PhD thesis. Department of Civil and Environmental Engineering, MIT, Cambridge, MA; 2002.
[4] Lysmer J, Kuhlemeyer RL. Finite dynamic model for infinite media. J Eng Mech Div-ASCE 1969;95(EM4):859–77.
[5] Lin G, Han Z, Li J. An efficient approach for dynamic impedance of surface footing on layered half-space. Soil Dyn Earthquake Eng 2013;49:39–51.
[6] Oliveira Barbosa JM, Park J, Kausel E. Perfectly matched layers in the thin layer method. Comput Methods Appl Mech Eng 2012;217–220:262–74.
[7] Ceballos M, Prato C. Experimental estimation of soil profiles through spatial phases analysis of surface waves. Soil Dyn Earthquake Eng 2011;31:91–103.
[8] Wolf JP. Foundation vibration analysis using simple physical models. Englewood Cliffs, NJ: Prentice-Hall; 1994.
[9] Theoretical and experimental modal analysis. In: Maia NMM, Silva JMM, editors. England: Research Studies Press Ltd; 1997.
[10] Watson GN. A treatise on the theory of Bessel functions. 2nd ed. Cambridge University Press; 1944.
[11] Kausel E. Early history of soil–structure interaction. Soil Dyn Earthquake Eng 2010;30:822–32.
[12] Ewing WM, Jardetzky WS, Press F. Elastic waves in layered media. NY: McGraw-Hill; 1957.
[13] Handbook of mathematical functions. In: Abramowitz M, Stegun I, editors. Washington DC: National Bureau of Standards; 1964.
[14] Hemsley JA. Elastic analysis of raft foundations. London: Thomas Telford,; 1998.
[15] Kausel E. Fundamental solutions in elastodynamics: a compendium. UK. Cambridge: University Press; 2006.
[16] Lysmer, J. Vertical motion of rigid footings, US Army Engineer Waterways Experiment Station, Report no. 3-115, Vicksburg, Mississippi, 137 pp, 1965.
[17] Luco JE, Westman RA. Dynamic response of circular footings, report UCLA-ENG-7113, University of California, Los Angeles; 1971. 45 p.
[18] Veletsos AS, Wei YT. Lateral and rocking vibration of footings. J Soil Mech Found Div-ASCE, 97; 1971; 1227–48.
[19] Wei YT. Steady state response of certain foundation systems. PhD thesis. Rice University, Houston, Texas; 1971.
[20] SUPER SASSI/PC: Complete Dynamic Soil–Structure Interaction Analysis System on Personal Computers, Stevenson & Associates, Cleveland, OH; 1996.